NEANDC(E) - 192 "U"
Vol. III - EURATOM
INDC (EUR) - 11/G

COMMISSION OF THE EUROPEAN COMMUNITIES

JOINT RESEARCH CENTRE

CENTRAL BUREAU FOR NUCLEAR MEASUREMENTS

GEEL - BELGIUM

NUCLEAR DATA PROGRESS REPORT 1977

MARCH 1978

THIS REPORT WAS COMPILED BY E.D. WATTECAMPS

TABLE OF CONTENTS

----

1. FAST NEUTRON DATA

Determination of Excitation Function for the Threshold Reaction $^{103}Rh(n,n')^{103}Rh^m$

A. Paulsen, H. Liskien, R. Widera, F. Arnotte

For in-pile neutron spectrum measurements the reaction $^{103}Rh(n,n')^{103}Rh^m$ is of special interest due to its low-lying threshold at about 30 keV neutron energy. Since this reaction is made use of in the form of foil activation the cross section measurements are done best by the activation method.

Metallic Rh samples were irradiated with monoenergetic neutrons at the CBNM Van de Graaff accelerator and the induced activities were subsequently measured with X-ray detectors. Relative activation measurements have been carried out in steps of 100 keV neutron energy from threshold to 4 MeV making use of known angular distributions of the neutron source reactions $^7Li(p,n)$, $T(p,n)$, $D(d,n)$. The excitation function was additionally scanned in steps of 50 keV between 100 and 400 keV neutron energy. An absolute cross section determination was carried out at 1.8 MeV. The relative cross section measurements will be extended above 4 MeV and further absolute determinations are in preparation.

Cross Sections for the Threshold Reaction $^{115}In(n,n')^{115}In^m$ below 4 MeV Neutron Energy

H. Liskien, F. Arnotte, R. Widera, A. Paulsen

Threshold reactions leading to radioactive nuclei with convenient half-life and radiation are in use for reactor dosimetry. The reaction $^{115}In(n,n')^{115}In^m$ with its low threshold of 0.339 MeV and its product with 4.486 h half-life and 0.459 γ's per decay [1] has been widely used but the consistency and accuracy of the needed cross sections was insufficient. Early in 1976 and using the 3.7 MV Van de Graaff generator of CBNM we have taken data for this reaction up to 4 MeV neutron energy and had the intention to continue these measurements for higher neutron energies with the new 7 MV Van de Graaff generator to be installed. However, in the meantime data sets from Chalk River [2] and Argonne [3] and a new evaluation were published. As these data are essentially in agreement with each other and with our data we see no point in investing further effort in these determinations.

Making use of known angular distribution of neutron source reactions overlapping sections of the relative excitation function were determined which were fitted together by minimizing the scatter of results of each neutron energy. As source of monoenergetic neutrons the $T(p,n)^3He$ reaction at 2.5, 3.0, 3.5, 3.6 and 3.7 MeV proton energy and the $D(d,n)^3He$ reaction at 1.0 MeV deuteron energy were employed. Metallic samples of 99.99% purity 20 mm in diameter and 5 mm thick were suspended from a graduated horizontal circle of 159 mm diameter centered above the neutron source. To check the adjustment, samples were always mounted on both sides at symmetric positions relative to the ion beam direction. Emission angles were chosen so that the nominal neutron energy (that for the center of the sample) corresponded to multiples of 100 keV. A Monte Carlo calculation taking into account the target thickness, the irradiation geometry and the reaction kinematics was later used to determine the neutron spectrum seen by each sample. The final average neutron energy takes into account the variation of the cross section within the energy range of that spectrum. Typically three pairs of indium samples at each nominal neutron energy were irradiated during the total of 16 runs performed. Multiple scattering corrections were applied. Near threshold a major correction was necessary for the effect of high energy neutrons emitted in the forward hemisphere but scattered by the 0.3 mm silver backing of the T-Ti targets. This effect has been checked experimentally by suspending also a pair of samples under such an emission angle that all direct neutrons fall below threshold. The relative $^{115}In^m$-activities of the irradiated samples were determined by observing the 336 keV γ-line in a 6.3 cm^3 planar Ge(Li) detector. The stability of this detector was monitored using sources of ^{51}Cr, ^7Be, and ^{22}Na.

A minimum of two activity determinations was made for each sample within eight hours after irradiation. A half-life of (4.486 ± 0.004) h was used [1] to calculate decay factors. $^{115}In^m$-activity due to the reaction $^{115}In(n,p)^{115}Cd$ (54 h) was found negligible.

Above 700 keV neutron energy the uncertainty of the relative cross sections is ± 4.7%. This figure has been obtained by adding quadratically the uncertainty contributions. It is supported by the average reproducibility at each neutron energy which was found to be ± 1.3 % for irradiations using the same source condition, and ± 2.7 % if results from different source conditions are combined.
At 2.10 MeV neutron energy an absolute cross section determination was performed relative to the well-known n-p scattering cross section. The relative results were then normalized at this energy. As neutron source we used the $T(p,n)^3He$ reaction at 3 MeV. A 76 keV thick T-Ti target was bombarded with a 10 μA proton beam and the 0° neutron fluence determined with a methane filled proportional counter positioned 1 m from the source. In addition the neutron source was monitored with a directional long counter to determine corrections for the survival factor. Indium samples were mounted at ± 20.8° relative to the proton beam direction as described above. Also the activity determinations were performed as described above. The absolute detection efficiency was obtained with an $^{115}In^m$-source which was - concerning dimensions and material - equal to the used samples, but with the activity distributed homogeneously in the center plane. Corrections for this difference were determined experimentally by sandwiching the activity between indium layers of various thicknesses. The uncertainty of the absolute cross section at 2.10 MeV is ± 4.9 %. This number has been obtained by adding quadratically the uncertainty contributions.
There is perfect agreement with the data of Smith and Meadows [3]. Typically our results are 5 to 7% higher than those of Santry and Butler [2].
A paper for publication is in preparation.

REFERENCES

[1] H.H. HANSEN, E. DE ROOST, W. VAN DER EIJK, R. VANINBROUKX, Z. Physik 269 (1974) 155.

[2] D.C. SANTRY, J.P. BUTLER, Can. J. Phys. 54 (1976) 757 and AECL-5371.

[3] D.L. SMITH, J.W. MEADOWS, Nucl. sci. Eng. 60 (1976) 319 and ANL/NDM-14.

Status Report about some Activation, Hydrogen and Helium Producing Cross Sections of Structural Materials

A. Paulsen

As an invited paper a status report about activation, hydrogen and helium producing neutron cross sections of chromium, iron and nickel was prepared for the NENADC/NEACRP Specialists Meeting on Neutron Data of Structural Materials for Fast Reactors held at CBNM Geel, December 5-8, 1977.
Experimental cross sections for the activation of Cr, Fe and Ni by neutron capture were compiled in the energy range from 1 keV to 1 MeV. Partly they were obtained by averaging experimental high resolution data from prompt γ-detection measurements. Differential cross sections for (n,p) and (n,α) reactions in the energy region from threshold to 20 MeV (for inclusion of the 14 MeV data) were compiled for all isotopes of Cr, Fe and Ni which have a natural abundance higher than 4 %.
All experimental information is compared with evaluated data files (ENDF/B-IV and KEDAK 3).

Measurement of Ni(n,p) and Ni(n,α) Cross Sections

A. Paulsen, H. Liskien, F. Arnotte, R. Widera

The reaction chamber was used in test measurements at the 7 MV Van de Graaff accelerator of the CBNM. As neutron source the D(d,n) reaction was chosen at E_d = 5 MeV resulting in neutrons of 8.2 MeV energy at 0° relative to the deuteron bea direction. The sample was a foil of natural Ni of 6.6 mg/cm^2 thickness. Cross section measurements are done by direct comparison with the differential H(n,p)n cross section. For this purpose recoil protons from a 13 mg/cm^2 olyehtylene foil are observed in the 15° detector. The test runs showed immediately that the experimental geometry with the neutron-producing target as close as possible to the reaction chamber is impracticable.
The neutron and γ-ray induced count rates in the scintillators are so high that besides unacceptable high random coincidence rates even considerable photomultiplier gain shifts are strongly disturbing. Therefore an experimental geometry as indicated in Fig. 1.1 was chosen.

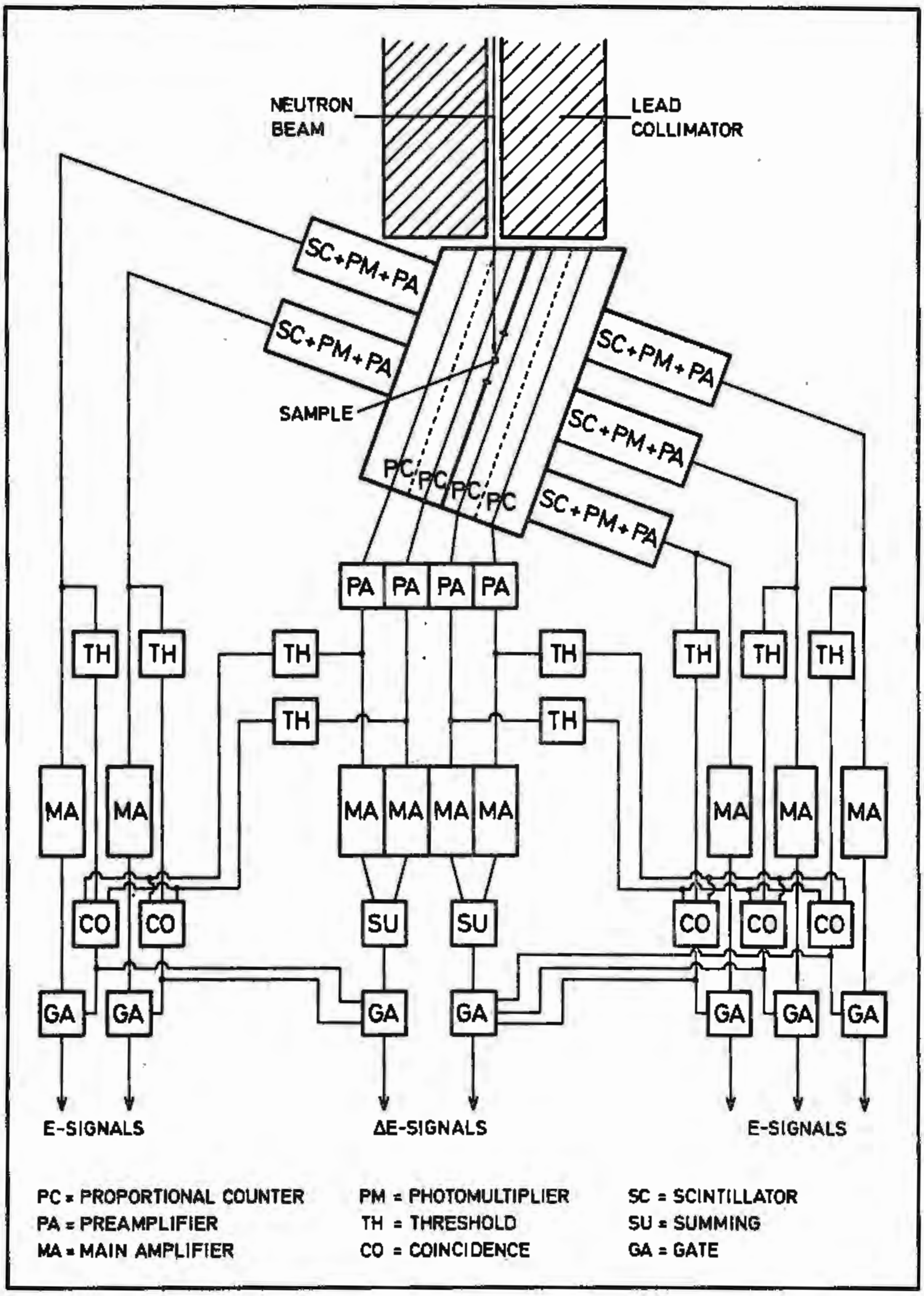

Fig. 1.1 Experimental set-up for reaction chamber.

A 20 cm long lead collimator is inserted between neutron-producing target and reaction chamber. This way the 2 mm thick CsI scintillators are sufficiently screened to arrive at acceptable single count and random coincidence rates. This changement on one hand reduces strongly the neutron intensity at the sample position but on the other hand improves considerably the background conditions so that it will probably permit a future use of surface barrier detectors in place of the scintillators.

The electronic circuitry used so far is indicated in Fig. 1.1 as a block diagram. With CO_2 as counting gas and some appropriate pulse shaping in the preamplifiers a coincidence resolution of 0.5 μs can be used. Some further pulse shaping in the main amplifiers (after generation of the timing signals by thresholds discriminators) compensates for the delays caused in the coincidence units, so that a proper gating is ensured without additional delay units.

Tests of bidimensional $E \times \Delta E$ analysis are promising with respect to an excellent separation of αparticles from protons but are delayed due to the late ordering of a multiparameter system of sufficient memory capacity caused by budgetary problems in 1977.

A typical E pulse height spectrum as obtained from the 15° detector looking at the recoil protons from the polyethylen radiator is shown in Fig. 1.2.

This spectrum was corrected by subtraction of two background runs: with the polyethylen radiator removed [1] and with the deuterium gas target evacuated [2]. The second background run corrects well for all spurious neutrons stemming from deuteron break-up. These neutrons are rather numerous at this deuteron energy as has been checked by TOF measurements.

A corresponding E pulse height spectrum of charged particles (p and α) from the nickel foil is shown in Fig. 1.3.

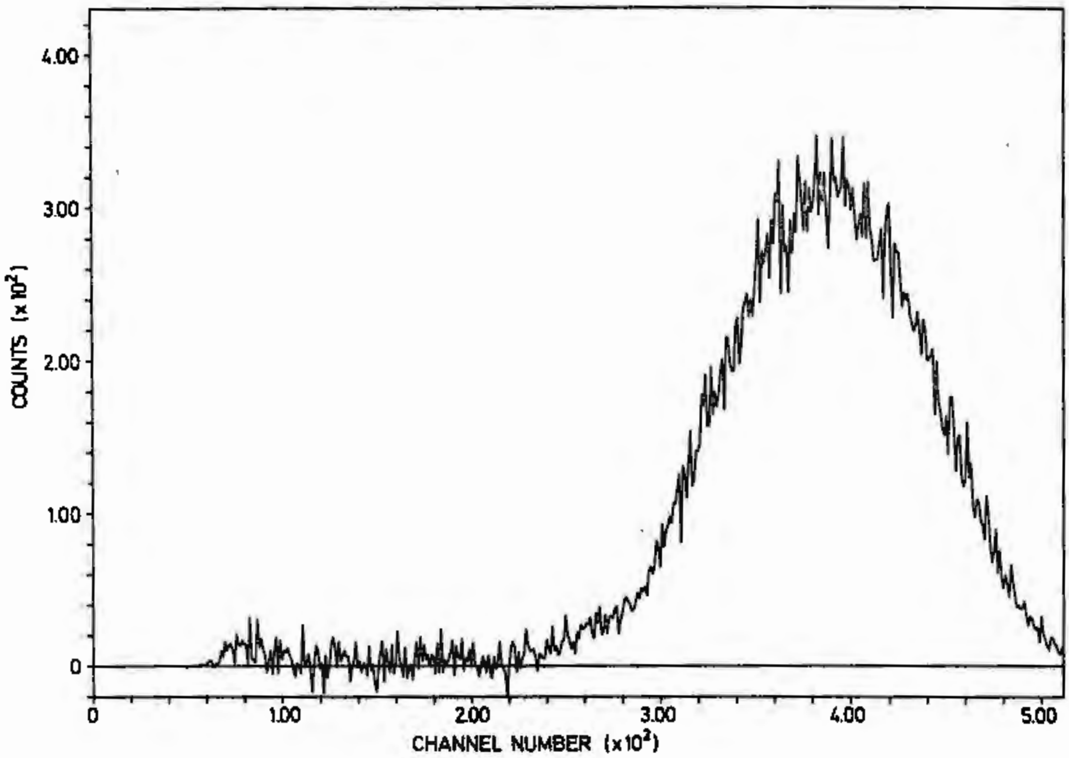

Fig. 1.2 Experimental pulse height spectrum of scintillation detector observing recoil protons from polyethylen radiator foil.

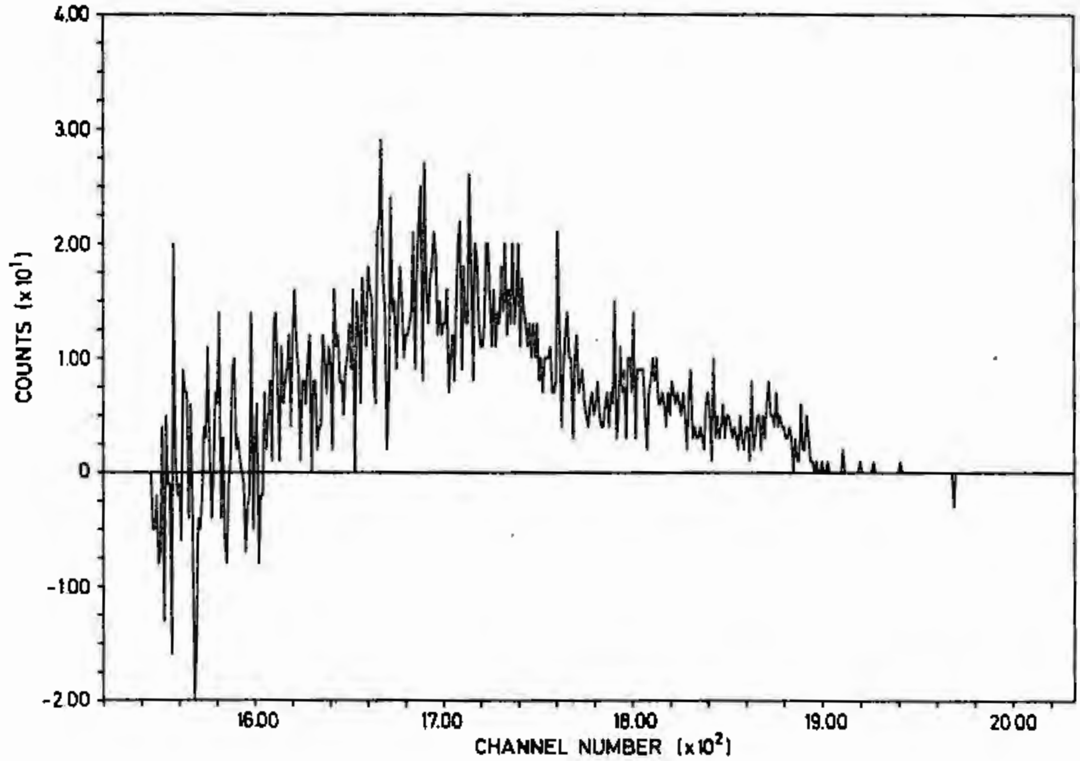

Fig. 1.3 Experimental pulse height spectrum of scintillation detector observing charged particles from nickel foil.

Again this spectrum was corrected by the two corresponding background runs as explained above. Just above threshold the larger statistical uncertainty caused by the background subtraction is clearly seen. Difficulties to be cleared up are connected with this low-energy cut-off of the measured spectrum which is influenced by unfavourable statistical conditions. Nevertheless a preliminary result can be evaluated from the measurement: $\sigma_{np+n\alpha}$(8.2 MeV) = 540 mb with a very rough estimate of a ± 10 % uncertainty. This compares well with a value of 550 mb to be calculated from assumed data in ENDF/B-IV and KEDAK 3 files.

Thick Target Neutron Yields from (α,n)-Reactions

H. Liskien, A. Paulsen, R. Widera, F. Arnotte

The goal is the determination of the number of neutrons per alpha for light elements (Z < 15) and for α energies covering the energy range up to 7 MeV. This information is needed for handling irradiated fuel and nuclear waste. n/α may be calculated from available differential (α,n)-cross sections and α stopping powers. More accurate data can be obtained from direct measurements using an electrostatic accelerator and a 4 π neutron detector with known efficiency curve.
Scanning of available literature revealed that thick target yields exist only for carbon and aluminium. However, much more information on thin target yields (cross section) are available. This information has been compiled and used together with evaluated α stopping powers to calculate the quantity n/α for all elements with Z < 15 with the exception of fluorine and sodium. Estimated uncertainties are ± 20 to ± 30 %. The results are given in Tab. 1.1 . A short paper has been published in Atomkernenergie 30 (1977)59.
The activity in this field has been continued by preparing series of measurements using the 7MV Van de Graaff accelerator of CBNM as source of monoenergetic αparticles (of variable energy) and a Cadarache "directional counter" as neutron detector. Tests with ^{27}Al(α,n) allowed to improve the target assembly with Faraday cup, which is needed to determine absolutely the αflux. Monte-Carlo calculations for the efficiency of the 4 π detector show that a neutron spectrum determination is indispensable to achieve an overall accuracy better than 5 %.

TABLE 1.1

The number of neutrons emitted per α-particle of energy E for the indicated elements (from Li to Si), and for the compounds UO_2 and UC

NEUTRONS / ALPHA												
E(MEV)	LI	BE	B	C	N	O	NE	MG	AL	SI	UO2	UC
0.1	---				---				---	---		
0.2	---				---				---	---		
0.3	---				---				---	---		
0.4	---		3.1E-09		---				---	---		
0.5	---		9.1E-09		---				---	---		
0.6	---		1.7E-08		---				---	---		
0.7	---		2.7E-08		---				---	---		
0.8	---		3.9E-08		---				---	---		
0.9	---		5.3E-08		---				---	---		
1.0	---		7.1E-08		---				---	---		
1.1	---		9.2E-08	4.2E-11	---				---	---		6.1E-12
1.2	---		1.2E-07	7.4E-11	---				---	---		1.1E-11
1.3	---		1.5E-07	1.1E-10	---				---	---		1.5E-11
1.4	---		1.9E-07	2.4E-10	---				---	---		3.4E-11
1.5	---	5.8E-09	2.4E-07	3.1E-10	---	1.8E-13			---	---	6.5E-14	4.4E-11
1.6	---	5.3E-08	3.1E-07	4.2E-10	---	2.7E-12			---	---	9.4E-13	6.0E-11
1.7	---	2.2E-07	4.0E-07	5.7E-10	---	2.8E-12			---	---	9.9E-13	7.9E-11
1.8	---	7.4E-07	5.1E-07	8.2E-10	---	4.3E-12			---		1.5E-12	1.1E-10
1.9	---	2.0E-06	6.3E-07	1.2E-09	---	2.1E-11	4.3E-11		---		7.1E-12	1.7E-10
2.0	---	3.5E-06	7.6E-07	2.0E-09	---	2.6E-11	1.8E-10		---		9.0E-12	2.7E-10
2.1	---	4.6E-06	9.0E-07	3.4E-09	---	3.4E-11	4.9E-10		---		1.1E-11	4.5E-10
2.2	---	5.6E-06	1.0E-06	5.3E-09	---	7.8E-11	6.5E-10		---		2.6E-11	6.8E-10
2.3	---	6.7E-06	1.2E-06	8.3E-09	---	1.1E-10	9.3E-10		---		3.4E-11	1.1E-09
2.4	---	7.7E-06	1.4E-06	1.1E-08	---	1.4E-10	1.3E-09		---	5.7E-10	4.6E-11	1.4E-09
2.5	---	8.8E-06	1.6E-06	1.3E-08	---	2.9E-10	1.9E-09		---	7.3E-10	9.6E-11	1.7E-09
2.6	---	1.0E-05	1.8E-06	1.5E-08	---	7.2E-10	2.9E-09		---	8.9E-10	2.3E-10	1.9E-09
2.7	---	1.1E-05	2.1E-06	1.7E-08	---	8.7E-10	5.3E-09		---	1.1E-09	2.8E-10	2.1E-09
2.8	---	1.2E-05	2.3E-06	1.8E-08	---	1.2E-09	7.3E-09		---	1.2E-09	3.8E-10	2.3E-09
2.9	---	1.3E-05	2.6E-06	2.0E-08	---	1.5E-09	1.1E-08		---	1.5E-09	4.8E-10	2.5E-09
3.0	---	1.4E-05	2.9E-06	2.1E-08	---	2.0E-09	1.4E-08	1.7E-08	---	1.7E-09	6.3E-10	2.6E-09
3.1	---	1.5E-05	3.2E-06	2.3E-08	---	2.2E-09	1.8E-08	2.0E-08		2.0E-09	7.0E-10	2.9E-09
3.2	---	1.6E-05	3.6E-06	2.5E-08	---	2.7E-09	2.0E-08	2.3E-08		2.4E-09	8.7E-10	3.1E-09
3.3	---	1.6E-05	4.1E-06	2.9E-08	---	3.3E-09	2.5E-08	2.7E-08	1.0E-10	2.9E-09	1.1E-09	3.5E-09
3.4	---	1.7E-05	4.6E-06	3.4E-08	---	4.0E-09	3.2E-08	3.3E-08	5.8E-10	3.5E-09	1.3E-09	4.1E-09
3.5	---	1.8E-05	5.2E-06	3.6E-08	---	4.5E-09	4.0E-08	4.0E-08	1.1E-09	4.2E-09	1.4E-09	4.3E-09
3.6	---	1.9E-05	6.0E-06	3.6E-08	---	6.0E-09	5.5E-08	4.8E-08	3.2E-09	5.1E-09	1.9E-09	4.4E-09
3.7	---	2.0E-05	6.8E-06	3.7E-08	---	7.6E-09	8.3E-08	5.8E-08	5.3E-09	6.1E-09	2.4E-09	4.4E-09
3.8	---	2.2E-05	7.8E-06	3.7E-08	---	9.1E-09	1.0E-07	7.0E-08	9.2E-09	7.3E-09	2.8E-09	4.5E-09
3.9	---	2.4E-05	8.8E-06	3.7E-08	---	1.1E-08	1.2E-07	8.4E-08	1.3E-08	8.7E-09	3.5E-09	4.5E-09
4.0	---	2.7E-05	1.0E-05	3.7E-08	---	1.3E-08	1.4E-07	1.0E-07	1.9E-08	1.0E-08	4.0E-09	4.5E-09
4.1	---	3.1E-05	1.1E-05	3.8E-08	---	1.4E-08	1.6E-07	1.2E-07	2.5E-08	1.4E-08	4.4E-09	4.5E-09
4.2	---	3.5E-05	1.3E-05	3.8E-08	---	1.6E-08	2.0E-07	1.5E-07	3.7E-08	1.7E-08	4.9E-09	4.6E-09
4.3	---	3.9E-05	1.4E-05	3.9E-08	---	1.9E-08	2.4E-07	1.8E-07	4.9E-08	2.1E-08	5.6E-09	4.6E-09
4.4	2.9E-09	4.3E-05	1.5E-05	4.1E-08	---	2.2E-08	2.8E-07	2.2E-07	6.8E-08	2.5E-08	6.6E-09	4.8E-09
4.5	3.7E-08	4.7E-05	1.7E-05	4.2E-08	---	2.4E-08	3.4E-07	2.7E-07	8.7E-08	3.1E-08	7.2E-09	5.0E-09
4.6	1.0E-07	5.1E-05	1.8E-05	4.4E-08	---	2.6E-08	4.0E-07	3.2E-07	1.2E-07	3.9E-08	8.1E-09	5.2E-09
4.7	2.0E-07	5.5E-05	1.9E-05	4.6E-08	---	2.9E-08	4.6E-07	3.8E-07	1.4E-07		8.9E-09	5.4E-09
4.8	3.4E-07	5.9E-05	2.1E-05	4.7E-08	---	3.1E-08	5.1E-07	4.4E-07	1.9E-07		9.5E-09	5.6E-09
4.9	5.0E-07	6.4E-05	2.3E-05	4.9E-08	---	3.4E-08	5.5E-07	5.1E-07	2.3E-07		1.0E-08	5.8E-09
5.0	7.1E-07	6.9E-05	2.4E-05	5.3E-08	---	3.6E-08	6.1E-07	5.8E-07	2.9E-07		1.1E-08	6.2E-09
5.1	9.9E-07	7.4E-05	2.6E-05	6.1E-08	---	3.8E-08	6.7E-07		3.6E-07		1.2E-08	7.0E-09
5.2	1.3E-06	8.0E-05	2.8E-05	6.9E-08	---	4.1E-08			4.3E-07		1.3E-08	8.0E-09
5.3	1.6E-06	8.6E-05		8.1E-08	---	4.5E-08			5.2E-07		1.3E-08	9.2E-09
5.4	1.9E-06	9.2E-05		9.2E-08	---	4.8E-08			6.2E-07		1.5E-08	1.0E-08
5.5	2.2E-06	9.8E-05		1.1E-07	---	5.1E-08			7.4E-07		1.5E-08	1.2E-08
5.6	2.6E-06	1.0E-04		1.2E-07	---	5.4E-08			8.6E-07		1.6E-08	
5.7	3.0E-06	1.1E-04		1.3E-07	---	5.7E-08			1.0E-06		1.7E-08	
5.8	3.6E-06	1.2E-04		1.5E-07	---	6.0E-08			1.1E-06		1.8E-08	
5.9	4.1E-06	1.3E-04		1.6E-07	---	6.3E-08			1.3E-06		1.9E-08	
6.0	4.8E-06	1.3E-04		1.7E-07	---	6.7E-08			1.5E-06		2.0E-08	
6.1	5.6E-06	1.4E-04		1.9E-07	1.2E-09	7.0E-08			1.7E-06		2.1E-08	
6.2	6.5E-06	1.5E-04		2.0E-07	3.6E-08	7.3E-08			2.0E-06		2.2E-08	
6.3	7.6E-06	1.5E-04		2.2E-07	1.2E-07	7.7E-08			2.3E-06		2.3E-08	
6.4	8.7E-06	1.6E-04		2.3E-07	2.3E-07	8.1E-08			2.6E-06		2.4E-08	
6.5	1.0E-05	1.7E-04		2.5E-07	3.4E-07	8.4E-08			2.9E-06		2.5E-08	
6.6	1.2E-05	1.7E-04		2.7E-07	5.9E-07	8.9E-08			3.3E-06		2.6E-08	
6.7	1.3E-05	1.8E-04		2.9E-07	9.4E-07	9.3E-08			3.7E-06		2.8E-08	
6.8	1.6E-05	1.9E-04		3.0E-07	1.3E-06	9.7E-08			4.0E-06		2.9E-08	
6.9	1.8E-05	2.0E-04		3.2E-07	1.5E-06	1.0E-07			4.5E-06		3.0E-08	
7.0	2.1E-05	2.0E-04		3.4E-07	1.8E-06	1.1E-07			4.9E-06		3.1E-06	

2. RESONANCE NEUTRON DATA

Cross Section Measurements on Fe

A. Brusegan, E. Cornelis**, F. Corvi, L. Mewissen*, G. Pasquariello, F. Poortmans*, G. Rohr, R. Shelley, T. van der Veen

Scattering measurements have been performed on a thin natural Fe sample ($n = 4.342\ 10^{-3}$ at/b) in the energy range between 1 keV and 300 keV. The experiments were performed on a 30 meter flight path station using ^{3}He gaseous scintillators as neutron detectors. The detectors were mounted at an angle of 135° relative to the neutron beam axis. It has been possible to assign l-values for a limited number of neutron resonances from these data. The experiments will be repeated on a 60 meter flight path station. The aim of these experiments is to assign spin and parity of neutron resonances from the analysis of neutron differential scattering data measured at various angles.

Precise transmission measurements were performed for the 1.15 keV resonance of ^{56}Fe. Resonance parameters for this resonance are requested for Doppler-coefficient calculations in fast reactors.

The experiments were performed at a 60 meter flight path station. The sample ($n = 7.60\ 10^{-3}$ at/b) was cooled down to liquid nitrogen temperature in order to reduce the effect of Doppler broadening. A shape analysis of the data has yielded the following results for the resonance parameters

$$\Gamma_n = 51 \pm 1.6 \text{ meV}$$

$$\Gamma_\gamma = 785 \pm 100 \text{ meV}$$

Fig. 2.1 shows the result of the shape analysis.

We have used the gas-model approximation for the calculation of the Doppler width Δ. Taking a Debye temperature of 467°K, the effective temperature in this gas model is 181°K. The value for the capture width Γ_γ is very dependent on the knowledge of Δ. An analysis of the data with various values for the effective temperature has shown that a change of 10% of the effective temperature changes the Γ_γ value by 12% and the neutron width Γ_n value by 1%.

---

* S.C.K.-C.E.N., Mol, Belgium

** R.U.C.A., University of Antwerp, Belgium

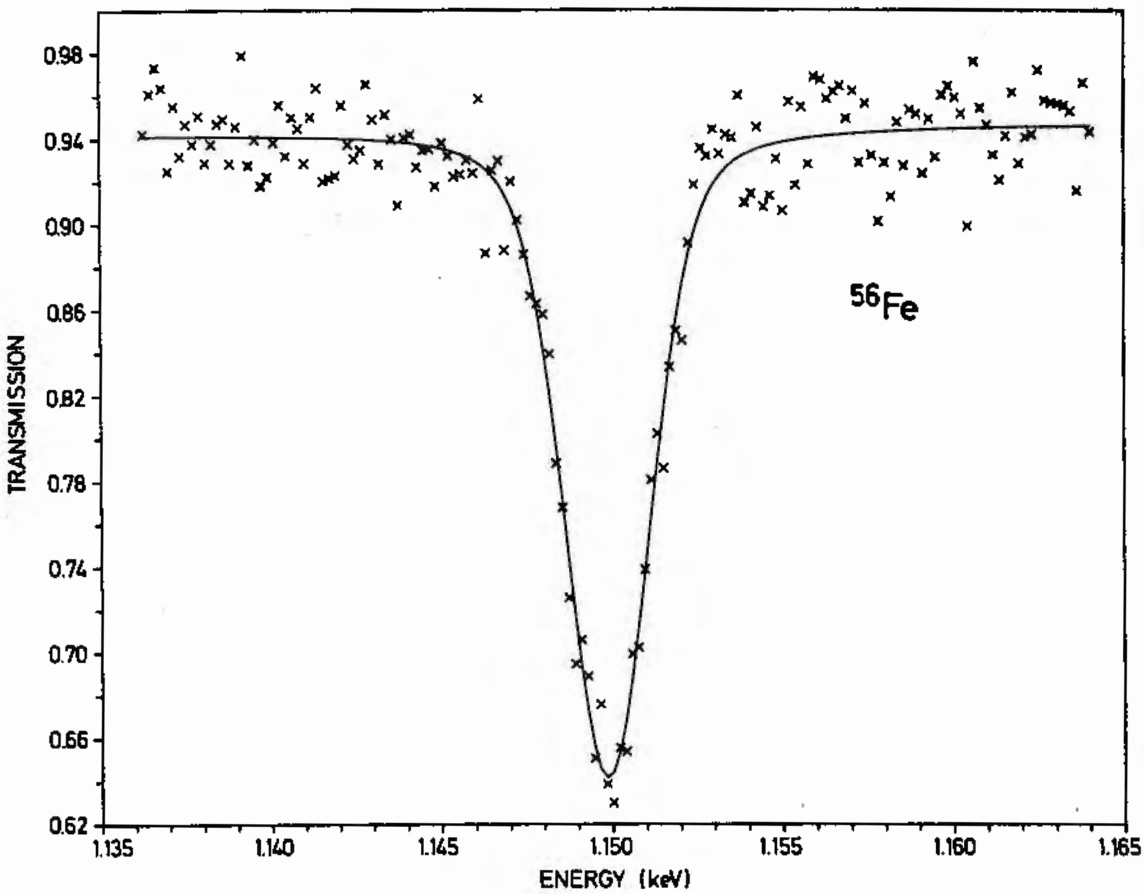

0.98
0.94
0.90
0.86
0.82
0.78
0.74
0.70
0.66
0.62
TRANSMISSION
1.135
1.140
1.145
1.150
1.155
1.160
1.165
ENERGY (keV)
^{56}Fe

Fig. 2.1

High resolution <u>capture cross section</u> measurements on enriched isotopes of ^{54}Fe and ^{56}Fe have been started, with the upgrated linac of 4 ns pulse width, at a 60 m station.

The C_6F_6 liquid scintillators used previously for detecting the capture γ-rays have been replaced by C_6D_6 liquid scintillators, which are encapsulated in a specially fabricated thin aluminium container in order to reduce the neutron detection sensitivity of the detector system. In a C_6F_6 detector scattered neutrons are captured especially in the resonances of fluorine at 27, 40 and 97 keV.

The C_6D_6 detectors have not constituants with a resonance behaviour in the neutron energy range of interest, which is particularly important for the measurement of the capture cross section of structural materials, where the ratio of scattering to capture in some s-wave resonances is of the order of 10^4.

The events are weighted according to the measured pulse height to achieve a detector response proportional to the total energy released in the capture process.

The measurements have been performed in the energy range 0.5 - 600 keV using oxide samples with a nominal thickness of n = 0.015 at/barn for ^{56}Fe and n = 0.0098 at/barn for ^{54}Fe.

The energy dependence of the neutron flux was measured with a 0.5 mm thick Li-glass detector as well as with a 3 mm sintered boron-carbide slab viewed by C_6D_6 detectors. In the latter case the capture sample has been replaced by the boron slab, measuring thus the neutron flux under the same geometrical condition as the capture cross section. The normalization of the capture data was done by observing capture in "black resonances" of Ag below 70 eV.

1.165 In Fig. 2.2 a part of our ^{56}Fe data in the energy range 345-370 keV has been plotted together with results obtained at the Oak Ridge linac. The asymmetric resonance seen in the Oak Ridge data at a neutron energy of 350 keV is in our data partly resolved into two resonances, indicating a better resolution mainly due to the longer flight path we have used. The higher ORNL cross section between the resonances 353 keV and 356 keV cannot be explained by the resolution effect only; it indicates a distortion probably due to differences in the neutron sensitivity of the detectors. This effect is much more pronounced in the Oak Ridge data for the 147.5 keV resonance shown in Fig. 2.3. The dotted curve (ORNL) describes the estimated contribution of neutrons scattered by the sample and captured in the detector system. This parasitic effect seems to be strongly reduced in our data if we compare

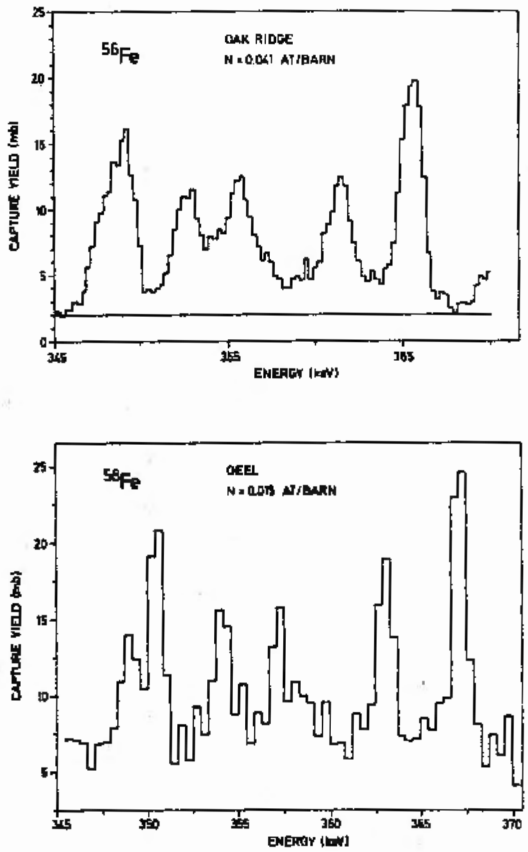

56Fe
OAK RIDGE
N = 0.041 AT/BARN
CAPTURE YIELD (mb)
ENERGY (keV)
56Fe
GEEL
N = 0.015 AT/BARN
CAPTURE YIELD (mb)
ENERGY (keV)

Fig. 2.2

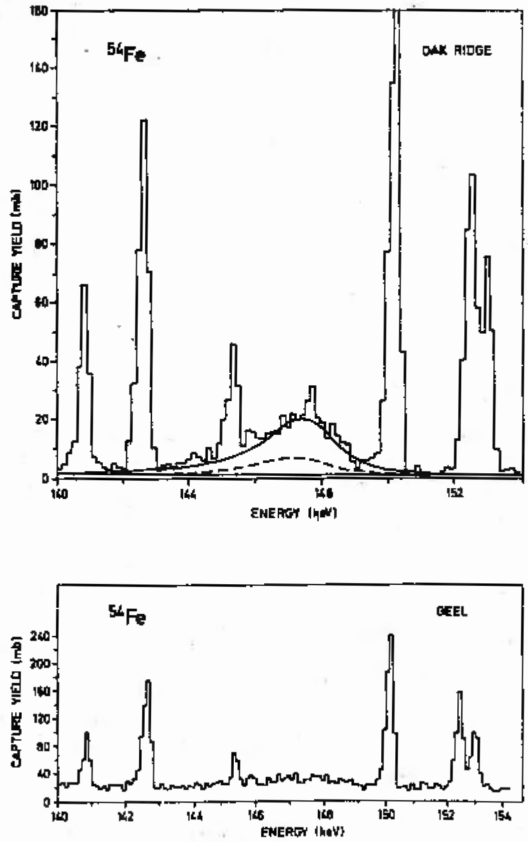

54Fe
OAK RIDGE
CAPTURE YIELD (mb)
ENERGY (keV)
54Fe
GEEL
CAPTURE YIELD (mb)
ENERGY (keV)

Fig. 2.3

the resonance area (or peak) with nearby resonances. The background in our data is higher by a factor of about 3, which can be partly explained by the longer flight path we have used. But additional measurements performed without a moderator at the target, thus producing only high energy neutrons, have shown that it will be possible to reduce the background by a factor of two using very thick overlap filters. Before starting with final measurements, we will try to measure the neutron sensitivity of the detector and will perform some more neutron flux studies at higher neutron energies.

Neutron Resonance Studies of ^{127}I

G. Rohr, R. Shelley, A. Brusegan

Iodine is one of the few fission products that is mono-isotopic. Its neutron data are important in "burn-up" calculations for nuclear reactors and it is also considered as a possible standard of integral measurements. Only transmission measurements extending to a neutron energy of 4 keV are reported in the literature.
In the present work capture, self-indication and transmission measurements have been performed and, in addition, a procedure enabling us to discriminate s- from p-wave resonances. From the data of these experiments we have determined resonance energies, neutron widths, level spacings, s-wave strength function and, for the first time, radiative widths and the p-wave strength function. In total 189 resonances have been analysed.
Neutron time-of-flight measurements were performed at the CBNM 60-MeV LINAC with a pulse width of 23 ns and a flight path of 60 meters. The characteristics of the three PbI_2 samples used and neutron energy ranges are given below in the discussion of each individual measurement. The detection system consisted of a pair of cylindrical C_6F_6 hydrogen-free liquid scintillators, each with a diameter of 4 inches and a length of 3 inches, the faces of which were in optical contact with RCA photomultipliers. The capture measurement was done with a sample thickness of 2.485×10^{-3} atoms/barn and covered the energy range from 20 eV to 5 keV with a nominal resolution varying between 0.5 and 5.3 ns/m in different energy ranges.

The data have been taken in two parameters, 13 time-of-flight and 7 amplitude bits, stored event by event on magnetic tape and off-line weighted over eight amplitude windows using the Maier-Leibnitz method. Absolute calibration was obtained by the "black resonance technique" using five resonances in Ag, at 16, 30, 51, 55 and 71 eV, with a sample thickness of 2.93×10^{-3} atoms/barn. The neutron flux was measured with a ^{10}B slab in place of the capture sample and with the same C_6F_6 detectors.

For the two self-indication measurements, done with sample thicknesses of 7.438×10^{-3} and 1.236×10^{-2} atoms/barn, the detection system (C_6F_6), capture sample and energy range were the same as in the capture measurement. The transmission measurement was performed with three different sample thicknesses, 2.485×10^{-3}, 7.438×10^{-3} and 1.236×10^{-2} atoms/barn, over the energy range from 20 eV to 2 keV. The detection system again consisted of C_6F_6 detectors with the ^{10}B slab and the background was determined using W, Mo, Co and Na black resonance filters.

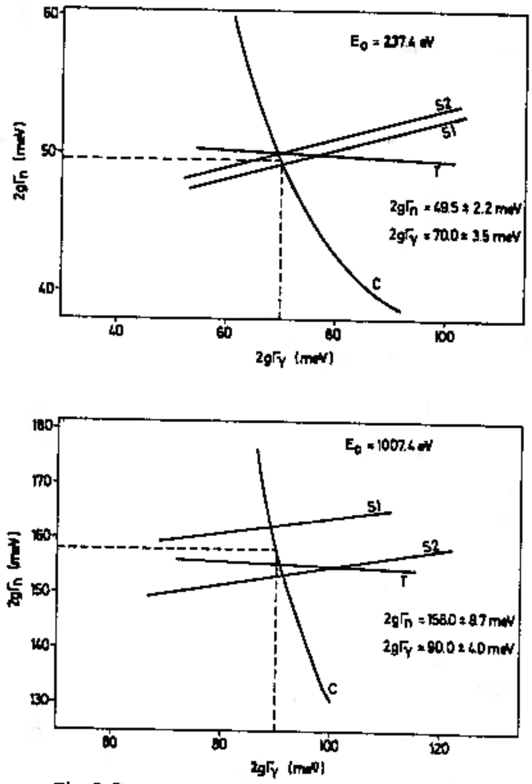

Fig. 2.5 Examples of resonance parameter analysis for two resonances of ^{127}I. The curves labelled C, T, S1 and S2 are from capture, transmission, self-indication (thin sample) and self-indication (thick sample) experiments respectively.

The capture and self-indication-ratio data have been analysed using a modified TACASI area analysis computer program which includes corrections for Doppler and resolution effects. The influence of multiple scattering on the capture area is taken into account by means of a Monte Carlo routine. A typical result obtained by this program is shown in Fig. 2.5.

Using the two parameter capture data we have attempted a parity assignment of the resonances by comparing the resonance areas of the time-of-flight spectrum taken with a high (5 MeV) and with a low (220 keV) amplitude bias. As a level scheme of the compound nucleus ^{127}I+n is not well known, the following procedure has been used to discriminate between s- and p-wave resonances. The resonances were divided into two groups, firstly those resonances with $2g\Gamma_n^o \geq 0.3$ and secondly those with $2g\Gamma_n^o < 0.3$. In the first group all resonances have been assigned as s-wave resonances and are seen to have (except in one case) an R value less than 0.075. In the second group all resonances with $R-\Delta R \geq 0.075$ are assigned as p-wave resonances, the high R values indicating that there are more possible dipole transitions ending at states of low energy with a positive parity.

In total the $2g\Gamma_n$ values of 189 resonances have been obtained in the energy range 20 to 2020 eV. From these resonances the s-wave strength function has been determined as $S_o = (0.80 \pm 0.09) \times 10^{-4}$ where any error introduced by the inclusion of unassigned p-wave levels is very small and has been neglected. The s-wave level spacing has been obtained by a best fit of the width distribution with a Porter-Thomas distribution for $2g\Gamma_n^o > 0.3$ meV, giving $D_o = 13.3 \pm 1.0$ meV.

To determine the p-wave strength function S_1 the value $\Sigma\, 2g\Gamma_n^o$ has been corrected by 18% to account for missed levels, assuming that resonances with $2g\Gamma_n^1 < 15$ meV escape detection. Hence $S_1 = \Sigma\, 2g\Gamma_n^1/(3 \cdot \Delta E \cdot F \cdot \epsilon)$ where $F(=0.75)$ is the correction factor due to the energy intervals covered by strong s-wave resonances. The correction factor $\epsilon\,(= 0.5)$ is the efficiency of the p-wave resonance assignment.

The final value for S_1 then becomes (3.4 ± 1.4). This value was checked by fitting the neutron width distribution of all resonances, with a superposition of a Porter-Thomas distribution for the s-wave resonances together with both a Porter-Thomas distribution and a chi-square distribution (with degree of freedom $\nu = 2$) for p-wave resonances. The fit was performed with the s-wave threshold again at $2g\Gamma_n^o = 0.3$ meV and with the lower threshold at $2g\Gamma_n^o = 0.02$ meV, the result of which was in very good agreement with the previous method for determining S_1.

For 76 broad resonances ($\Gamma_n \geq \Gamma_\gamma$), $2g\Gamma_\gamma$ has been determined but in five cases, where the value obtained is seen to be exceptionally high, doublets are assumed. The remaining 71 resonances give an average value $2g\Gamma_\gamma$ = 82 meV which is considerably smaller than the value of 130 meV indicated from systematics.
To obtain the final $2g\Gamma_\gamma$ value, the 16 well isolated resonances which gave the best cutting points in the $\Gamma_n - \Gamma_\gamma$ plane were used. These gave a value of $2g\Gamma_\gamma$ = (86.0 ± 9.0)meV where the uncertainty includes both a systematic error and an error due to the fact that the relative number of resonances in the two spin states is not known.

Measurement of the Fission Cross Section of ^{232}Th

J. Blons+, D. Paya+, M. Ribrag+, C. Mazur+, H. Weigmann

In a collaboration with a group from CEA-Saclay measurements of the ^{232}Th fission cross section have been started. Apart from its practical importance for fast reactors operating on the ^{232}Th-^{233}U fuel cycle, this cross section is of prime interest from a fundamental physical point of view. In the region around 1.6 MeV neutron energy, i.e. a few hundred keV below the fission threshold, the $^{232}Th(n,f)$ cross section is dominated by two strong resonances which are attributed to vibrational states of the strongly deformed compound nucleus ^{233}Th. In earlier experiments of Blons et al. (Phys. Rev. Lett. 35 (1975) 1749) at Saclay it had been shown that these two strong resonances show a fine structure which possibly can be explained by rotational bands built upon the vibrational states. Such a simple structure would allow to obtain information on the deformation potential of the fissioning ^{233}Th nucleus from the $^{232}Th(n,f)$ cross section data. It turned out, however, that for a quantitative analysis data of still higher resolution would be necessary. Therefore, the main objective at the present investigation is to measure the $^{232}Th(n,f)$ cross section with very high neutron energy resolution of about 2 keV -FWHM) at 1.6 MeV. A 100 m flight path was chosen and the linear accelerator was operated at its minimum burst width of 4 nsec. The detector is a gazeous scintillator which is separated into six individual cells, loaded with 6.6 g (in total) of ^{232}Th and 1.2 g of ^{237}Np for normalization. Time of flight spectra are taken separately for each of the six cells and added after correction for different flight path lenghts.

+ CEA - CEN de Saclay

Fig. 2.6 shows a spectrum obtained that way where the region around the 1.6 MeV vibrational resonance is displayed. The considerable amount of fine structure is clearly visible.

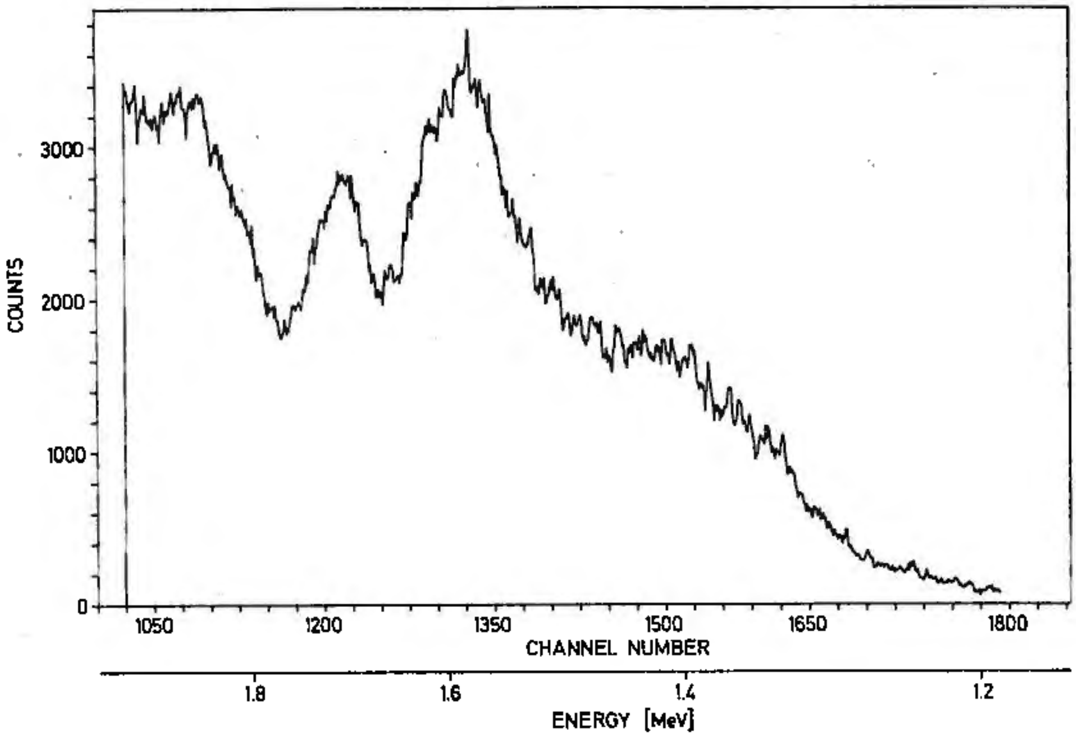

Fig.2.6 Fission yield of ^{232}Th.

The measurements on this nucleus have practically been finished. Analysis of the data will be started in the following months. Also, a similar measurement (using a 50 m flight path) on ^{230}Th will be done in 1978.

<u>Measurement of the Fission cross section of ^{235}U</u>

R. Barthélémy, C. Wagemans

Although ^{235}U is an extensively studied nucleus, the accuracy of its neutron induced fission cross section remains unsatisfactory. Even between the most recent measurements discrepancies up to 10 per cent exist. Especially in the eV and keV neutron energy region such a situation is very astonishing, since here the fission cross section is rather high and also the neutron flux determination is expected to be straightforward.
However, since σ_f measurements relative to a ^{6}Li flux monitor tended to result in lower σ_f values, we remeasured the ^{235}U fission cross section relative to $^{10}B(n,\alpha)$ and to $^{6}Li(n,\alpha)$ independently. Surface barrier detectors

and back-to-back foils were used, which has the advantage that fission fragments and neutron flux are detected at the same time and from the same position in the neutron beam.

The measurements were done at an 8m flight path and neutron energies from 0.015 eV up to a few keV were covered. Since manganese was used as a permanent neutron filter, the useful energy region was 0.015 - 200 eV.

So two σ_f-measurements were performed with the same apparatus and under identical conditions, the only difference being the thin ^{10}B or ^{6}Li foil used for the neutron flux determination.

The fission cross section values obtained from both measurements were consistent within the experimental accuracy. Also the boron-to-lithium ratio was obtained during these measurements. It was compatible with a $^{1}/v$-behaviour of both $^{6}Li(n,\alpha)$ and $^{10}B(n,\alpha_0 + \alpha_1)$ reaction cross sections, as expected. So the present measurements allow to conclude that for low neutron energies differences of several per cent in σ_f cannot be due to the neutron flux standard used, if the thin foil method is applied.

These measurements will be continued to higher neutron energies (30 keV).

The 6.67 eV Resonance in $^{238}U + n$

P. Staveloz*, L. Mewissen*, C. Cornelis**, F. Poortmans*

The extensive studies on neutron interactions with the ^{238}U nucleus have been completed by complementary measurements on the 6.67 eV resonance which is of particular importance for thermal reactor design.

Table 2.1. shows the results for the resonance parameters of the 6.67 eV resonance obtained from previous measurements.

TABLE 2.1

Resonance Parameters for 6.67 eV resonance

Γ_n (MeV)	Γ_γ (MeV)	Quantity measured	Author	Year
1.52 $\pm$ 0.07	(24)	σ_t	Harvey et al.	1955
1.4 $\pm$ 0.1	26.1 $\pm$ 1.5	σ_t	Lynn et al.	1955
1.54 $\pm$ 0.1	24 $\pm$ 2	σ_t	Levin et al.	1956
1.15 $\pm$ 0.04	21.15 $\pm$ 1.30	σ_t	Radkevich et al.	1957
1.45 $\pm$ 0.12	26.0 $\pm$ 3.0	σ_t	Bollinger et al.	1957
1.48 $\pm$ 0.05	25 $\pm$ 2	S.I	Rosen et al.	1960
1.52 $\pm$ 0.01	27.2 $\pm$ 1.5	σ_t	Jackson et al.	1962
1.578$\pm$ 0.106	23.43 $\pm$ 10.12	σ_γ, σ_s	Asghar et al.	1966
1.52 $\pm$ 0.05	(23.5)	σ_t, σ_γ, S.I.	Rahn et al.	1972
1.48 $\pm$ 0.032	23.0 $\pm$ 0.8	σ_t	Olsen et al.	1977
1.50 $\pm$ 0.03	21.8 $\pm$ 1	σ_t, S.I.,σ_γ	Liou et al.	1977
(1.50)	24.2 $\pm$ 0.8	σ_s	present result	1977

In most cases, these results were obtained from a shape analysis of transmission data or from an area analysis of transmission and self-indication data, measured with various sample thicknesses. In only one case, see Asghar et al., the resonance parameters were deduced from scattering and capture experiments, however with a very large error of about 40% on the capture width.
The resonance parameters quoted in the ENDF/B-IV evaluation were $\Gamma_n = 1.50$ meV and $\Gamma_\gamma = 25.6$ meV. In this evaluation, the largest weight was given to the results of Jackson and Lynn. These authors made a very careful study of the total cross section shapes measured at various sample temperatures. However, the evaluated parameters are not able to explain various integral experiments in thermal-neutron reactor fuel lattices. Especially, the effective or shielded resonance integrals, which are largely dependent on the capture width of the 6.67 eV resonance, are overpredicted by the evaluated resonance parameters.
As can be seen from Table 2.1 there is a good agreement on the values for Γ_n but the spread on Γ_γ is important.
We have deduced the capture width Γ_γ from an area analysis of a scattering cross section measurement supposing a known value for $\Gamma_n = 1.50$ meV.
An area analysis was performed in order to be less dependent on the Doppler width, which is, at room temperature, about twice the resonance width.
A very thin sample was used in order to have small corrections for multiple interactions of neutrons in the sample.
Fig. 2.7. shows the experimental scattering cross section for ^{238}U and the single-level Breit-Wigner curve calculated from the parameter mentioned above.

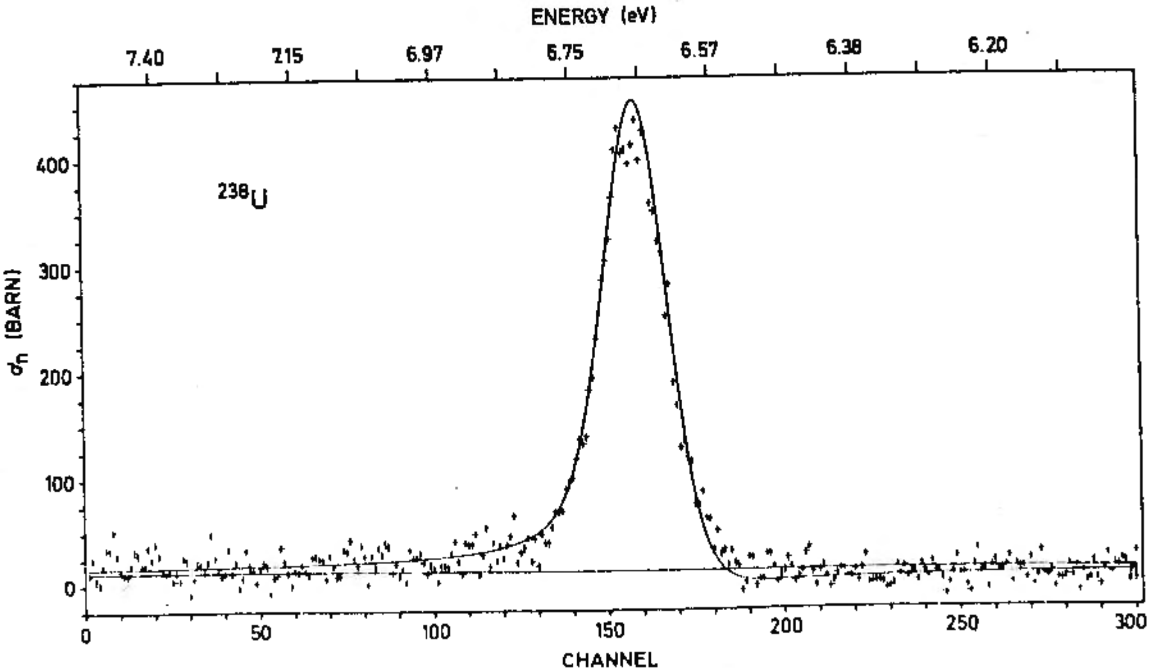

Fig. 2.7

Also shown on this figure is the least-squares fit to the base-line. The count rate, after substraction of the contribution of the 6.67 eV resonance is slowly varying in this small energy range. It was fitted to a function (a + b I), where a and b are constants and I stands for the channel number. The plotted line includes, apart from this function, the potential scattering cross section.

We have also checked how sensitive the results are to the value of the effective potential scattering radius (R) and to the Doppler width. R was assumed to be 0.94 10^{-12} cm and the effective temperature T_{eff} for the calculation of the Doppler width was 300°K. A variation of 10% on R and of 20% on T_{eff} had no detectable influence on the results of the area analysis.

Taking Γ_n = 1.50 meV, we find our area analysis : Γ_γ = 24.2 ± 0.8 meV.

Fig. 2.9 shows the value of Γ_n versus Γ_γ obtained from the area analysis of our scattering data. Also shown are the results of the three most precise previous measurements and the ENDF/B-IV value.

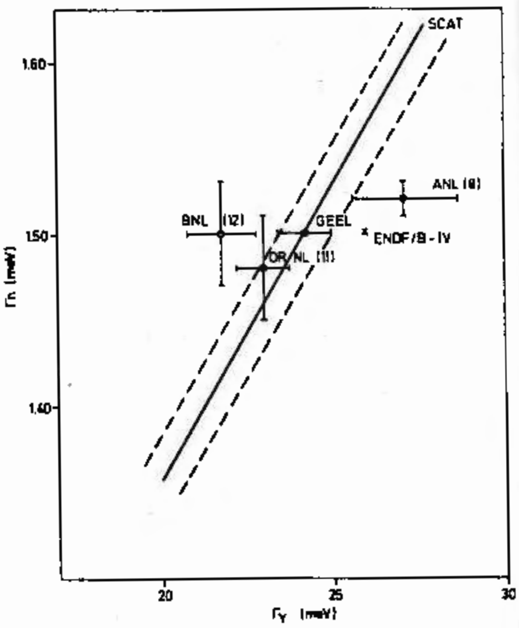

Fig.2.9

Our present scattering data agree with the results from Oak Ridge but not with those from Argonne and Brookhaven.

In low ^{235}U-enriched uranium lattices, the ratio of epithermal-to-thermal ^{238}U capture is over predicted by approximately 10% if one takes the ^{238}U resonance parameters from ENDF/B-IV. The discrepancies between the thermal reactor benchmark calculations, using differential data, and integral experiments can be removed if one reduces the effective resonance integral by about 1 barn. M. Bath has calculated the influence of the resonance parameters of the first four resolved s-wave resonances of ^{238}U on the effective resonance integral for the TRX-1 lattice (Report BNL-NCS-50451). With the same procedure we find that, for that lattice, the effective capture resonance integral is reduced by only 0.11 barn if the capture width is reduced from 25.6 meV (ENDF/B-IV value) to 24.2 meV (present result).

Neutron Resonance Parameters for ^{238}U

E. Cornelis**, L. Mewissen*, F. Poortmans*, G. Rohr; R. Shelley,
T. van der Veen

Because of the importance of ^{238}U resonance parameters and neutron cross sections in the resolved resonance region for thermal and fast reactors, many experiments have been performed in the past. There still remain, however, several discrepancies between the results of the various experiments, especially concerning the resonance parameters above 1 keV. Another problem is the inconsistency between the differential data and the results from integral experiments.

We have performed a series of total, capture and scattering cross section measurements using the neutron time-of-flight facility at the CBNM linear electron accelerator. These measurements were performed in the frame of a collaboration with SCK-CEN, Mol. The neutron widths have been obtained for more than 400 resonances below 4.3 keV and the total capture width for 73 resonances.

The transmissions were measured by alternating the sample in and out of the neutron beam every ten minutes. The automatic sample changer was located at 30 meters from the neutron target. The samples were cooled at liquid nitrogen temperature.

The scattering cross section was measured relative to Pb for which $\sigma_n = 11.28 \pm 0.06$ barn was used.

The capture detector system consisted of two C_6F_6 liquid scintillators. Pulse-height and time-of-flight were recorded simultaneously and a weighting was applied on the pulse height spectrum. The energy spectrum of the neutrons at the detector station was measured with a ^{10}B slab viewed by the C_6F_6 scintillators; the $^{10}B(n,\alpha)^7Li^*$ cross section was assumed to vary as $E^{-1/2}$ in the energy range of interest. The normalization of the capture data was done by observing capture in "black resonances" of Ag below 70 eV. The systematic error introduced by the normalization is supposed to be less than 2%. The result of this normalization is confirmed by the good agreement between the results from the transmission measurements and the capture measurements for small resonances ($\Gamma_n \ll \Gamma_\gamma$).

---

* SCK-CEN, Mol, Belgium

** R.U.C.A., University of Antwerp, Belgium

The transmission spectra were analysed using a modified Atta-Harvey code. Resonances were described using the single level Breit-Wigner formula. Shape analysis was limited to the low energy range where the spectrometer resolution was not involved; area analysis has been performed throughout the whole region. For the thickest samples interference effects become evident and a multilevel shape analysis program due to de Saussure, Olsen and Perez was used to analyze the data. In Fig. 2.10 an example of the resonance-resonance interference effect is shown: The single Breit-Wigner analysis is not able to describe correctly the interference effects.

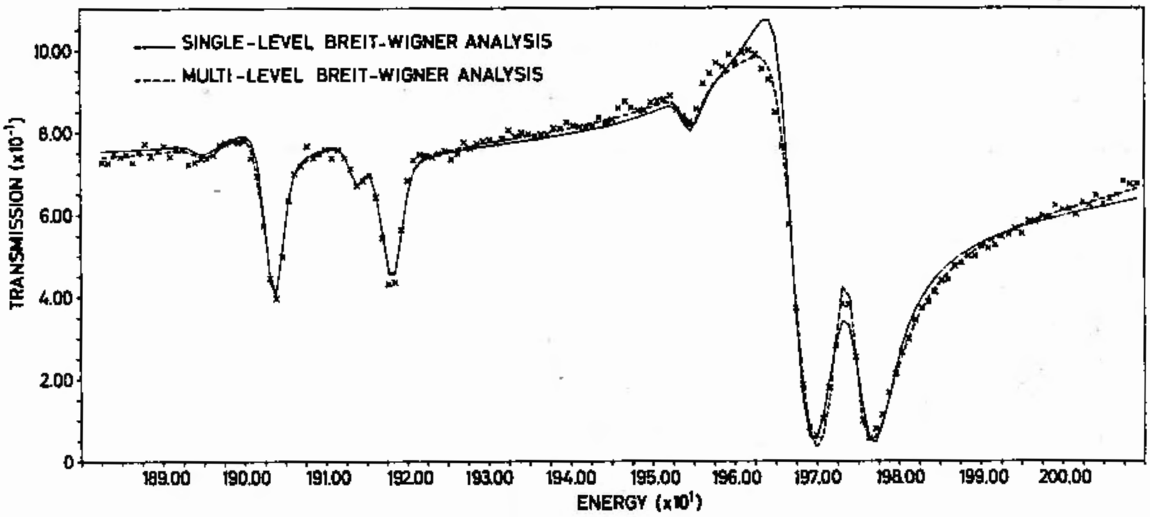

Fig.2.10 Comparison of single-level and multi-level Breit-Wigner analysis of neutron transmission through ^{238}U in the neutron energy range 1880 eV to 2010 eV.

The capture area analysis code TACASI was used to analyze the capture data. This code contains a Monte Carlo subroutine to determine the multiple interaction effects.

For the reduction of the scattering data a special code was written to fit the geometry of our experiment. After normalization and background corrections, the influence of selfscreening and multiple interaction was calculated using a Monte Carlo method. Finally the resonance parameters were obtained from a single level area analysis.

Most of the analysis has been completed now and we have obtained the neutron widths for more than 400 resonances below 4.3 keV neutron energy. The total capture width was obtained for 73 resonances.

From these data, we have deduced the following results for the average properties of s-wave neutron resonances:

Mean capture width:

$$\Gamma_\gamma = 23.60 \text{ meV} \pm 0.11 \text{ meV (stat.)} \pm 0.50 \text{ meV (syst. error)}$$

Neutron Resonance Parameters for ^{238}U

E. Cornelis[**], L. Mewissen[*], F. Poortmans[*], G. Rohr; R. Shelley, T. van der Veen

Because of the importance of ^{238}U resonance parameters and neutron cross sections in the resolved resonance region for thermal and fast reactors, many experiments have been performed in the past. There still remain, however, several discrepancies between the results of the various experiments, especially concerning the resonance parameters above 1 keV. Another problem is the inconsistency between the differential data and the results from integral experiments.

We have performed a series of total, capture and scattering cross section measurements using the neutron time-of-flight facility at the CBNM linear electron accelerator. These measurements were performed in the frame of a collaboration with SCK-CEN, Mol. The neutron widths have been obtained for more than 400 resonances below 4.3 keV and the total capture width for 73 resonances.

The transmissions were measured by alternating the sample in and out of the neutron beam every ten minutes. The automatic sample changer was located at 30 meters from the neutron target. The samples were cooled at liquid nitrogen temperature.

The scattering cross section was measured relative to Pb for which $\sigma_n = 11.28 \pm 0.06$ barn was used.

The capture detector system consisted of two C_6F_6 liquid scintillators. Pulse-height and time-of-flight were recorded simultaneously and a weighting was applied on the pulse height spectrum. The energy spectrum of the neutrons at the detector station was measured with a ^{10}B slab viewed by the C_6F_6 scintillators; the $^{10}B(n,\alpha)^7Li^*$ cross section was assumed to vary as $E^{-1/2}$ in the energy range of interest. The normalization of the capture data was done by observing capture in "black resonances" of Ag below 70 eV. The systematic error introduced by the normalization is supposed to be less than 2%. The result of this normalization is confirmed by the good agreement between the results from the transmission measurements and the capture measurements for small resonances ($\Gamma_n \ll \Gamma_\gamma$).

---

[*] SCK-CEN, Mol, Belgium

[**] R.U.C.A., University of Antwerp, Belgium

The transmission spectra were analysed using a modified Atta-Harvey code. Resonances were described using the single level Breit-Wigner formula. Shape analysis was limited to the low energy range where the spectrometer resolution was not involved; area analysis has been performed throughout the whole region. For the thickest samples interference effects become evident and a multilevel shape analysis program due to de Saussure, Olsen and Perez was used to analyze the data. In Fig. 2.10 an example of the resonance-resonance interference effect is shown: The single Breit-Wigner analysis is not able to describe correctly the interference effects.

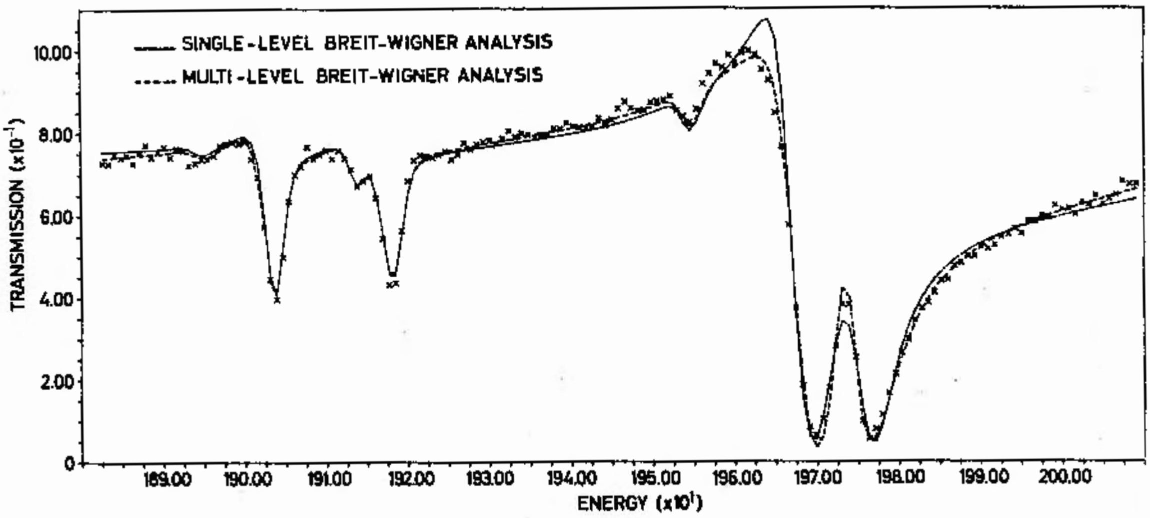

Fig.2.10 Comparison of single-level and multi-level Breit-Wigner analysis of neutron transmission through ^{238}U in the neutron energy range 1880 eV to 2010 eV.

The capture area analysis code TACASI was used to analyze the capture data. This code contains a Monte Carlo subroutine to determine the multiple interaction effects.

For the reduction of the scattering data a special code was written to fit the geometry of our experiment. After normalization and background corrections, the influence of selfscreening and multiple interaction was calculated using a Monte Carlo method. Finally the resonance parameters were obtained from a single level area analysis.

Most of the analysis has been completed now and we have obtained the neutron widths for more than 400 resonances below 4.3 keV neutron energy. The total capture width was obtained for 73 resonances.

From these data, we have deduced the following results for the average properties of s-wave neutron resonances:

Mean capture width:

$$\Gamma_\gamma = 23.60 \text{ meV} \pm 0.11 \text{ meV (stat.)} \pm 0.50 \text{ meV (syst. error)}$$

The distribution of the Γ_γ values around the mean value is very narrow, the dispersion being only 0.91 meV.

s-wave strength function:

$$S_o = (1.00 \pm 0.21)10^{-4} \text{ for the energy range 0–1000 eV}$$

$$S_o = (1.15 \pm 0.12)10^{-4} \text{ for the energy range 0–4260 eV.}$$

It is interesting to note that in the neutron energy range from 1.9 keV to 2.9 keV the strength function shows a particularly high "local" value of about 1.6 10^{-4}, 50% of which is due to only 6 resonances.

The mean level spacing D_o of s-wave resonances was deduced by fitting the reduced neutron width distribution to a Porter-Thomas distribution above a bias value Γ_n^o = 0.25 meV.

Fig. 2.11 shows the integral distribution of all reduced neutron widths. The full line represents the integral Porter-Thomas distribution which was obtained by fitting the experimental distribution above the bias value Γ_n^o = 0.25 meV. The surplus of resonances observed with smaller Γ_n^o-value is due to p-wave neutron interaction. From the fitted curve a total number of s-wave resonances of N_o = 196 is obtained for the energy range 0-4260 eV, which yields:

$$D_o = (22 \pm 1) \text{ eV.}$$

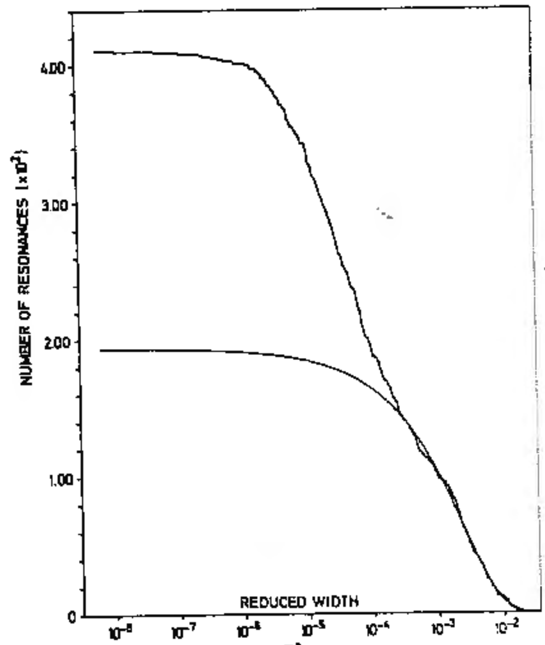

Fig. 2.11 Integral distribution of reduced neutron widths of ^{238}U resonances.

<u>Neutron Resonance Parameters for ^{237}Np</u>

A. Angeletti, E. Cornelis**, L. Mewissen*, F. Poortmans*, G. Rohr, T. van der Veen, G. Van Praet**, H. Weigmann

Total, scattering and capture cross section measurements were performed for ^{237}Np in the energy range between 8 eV and 204 eV. The main purpose of these experiments was to obtain a value for the mean capture width. For a few resonances it has been possible to obtain the resonance spin. The experiments have been performed on a 30 meter flight path station at the CBNM Linac neutron time-of-flight spectrometer in the frame of a collaboration with SCK-CEN Mol.

---

* SCK-CEN, Mol, Belgium

** R.U.C.A., University of Antwerp, Belgium

^3He gaseous scintillators were used as neutron detectors for the transmission and scattering experiments. The capture detector consisted of a pair of C_6F_6 scintillators. Pulse height and time-of-flight were recorded simultaneously and a weighting was applied on the pulse height spectrum. The samples were made of neptunium-oxide powder canned between 0.5 mm thick aluminium plate. Transmission experiments were performed on three sample thicknesses 1.78 10^{-3} atoms/barn, 5.33 10^{-3} atoms/barn and 2.36 10^{-2} atoms/barn. The sample for the scattering and capture experiments was 1.39 10^{-3} atoms/barn thick.
An area and shape analysis of the transmission data was performed using a modified version of the Atta-Harvey code. The capture data were analysed with the area analysis code of Fröhner and Haddad. The scattering data were corrected for multiple-interaction effects of scattered neutrons in the sample before performing the area analysis.
The neutron widths were deduced from the transmission and capture data. The results between the two experiments are in good agreement.
The capture width was obtained for 27 resonances below 50 eV by two methods:

1. From a shape analysis of the transmission data.
2. By a combined area analysis of the transmission data taken with the three sample thicknesses.

The parameters $g\Gamma_n$ and Γ_γ being known, the statistical weight factor g and so the resonance spin J could be determined for 10 resonances below 50 eV from an area analysis of the scattering data. The results are in agreement with those from polarization experiments by Keyworth et al.
Fig. 2.12 shows an example of such area analysis.

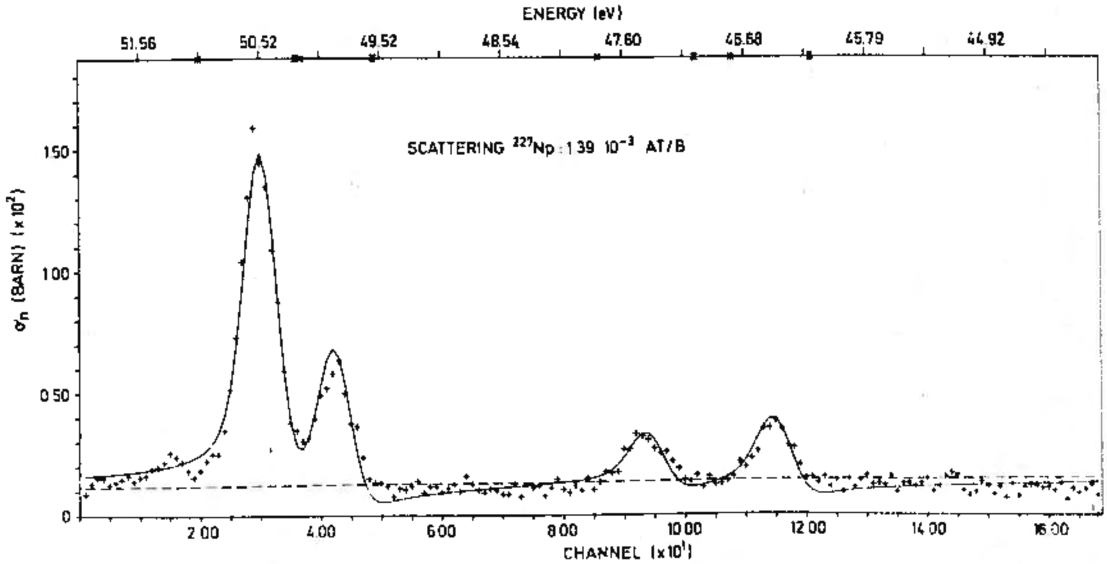

Fig 2.12 Scattering cross section of ^{237}Np between 44.5 eV and 51.6 eV neutron energy. The full curve represents the cross section calculated from the adopted resonance parameters

The parameter $g\Gamma_n$ was deduced for 213 resonances. The results are in agreement with those previously measured at Saclay. The s-wave strength function we obtained is:

$$S_o = (0.95 \pm 0.09) \cdot 10^{-4}.$$

The mean level spacing was deduced by fitting the distribution of reduced neutron widths with a Porter-Thomas distribution above a bias of $2\ g\Gamma_n^o = 0.04$ meV, which has yielded:

$$D_o = (0.74 \pm 0.03)\ \text{eV}.$$

The mean capture width for 27 resonances below 50 eV is:

$$\Gamma_\gamma = [41.2 \pm 0.5\ (\text{statist.}) \pm 1.0\ (\text{system.})]\ \text{meV}.$$

The fluctuations of Γ_γ around this mean value are small (standard deviation = 3 meV) except for three resonances at 38.3 eV, 39.0 eV and 40.0 eV respectively, for which Γ_γ is about 50% larger.

Kinetic Energy- and Mass-Distributions for ^{239}Pu(n,f)-fragment in the Resonance Region

R. Barthélémy, C. Wagemans*, G. Wegener-Penning, H. Weigmann

Fission fragment kinetic energy- and mass-distributions from ^{239}Pu(n,f) reaction were measured at GELINA in the neutron energy range from thermal up to about 100 eV. In this energy region several well isolated resonances with spin-values J = 0 and J = 1, are available, which allow a study of the mass- and energy-distributions in function of the resonance spin.
Fission fragments emitted by a thin Pu-layer (deposited on a very thin VYNS-support) were detected in two large surface-barrier detectors. These detectors were cooled and stabilised at 0°C, which made them insensitive to fluctuations of the room temperature. In this way a good long-term stability was obtained, which is necessary for measurements with a low counting-rate. Within the present experimental accuracy no striking differences between energy- and mass-distributions for both spin-states are observed. The measurements were temporarily interrupted due to radiation damage in the VYNS-support of the Pu-layer. They will be continued upon the receipt of a new sample.

Measurements of the ^{241}Am Neutron Induced Fission Cross Section in the Energy Range from 5 keV to 5 MeV using Van de Graaff Accelerator

C. Budtz-Jørgensen, H.-H. Knitter

The actinide ^{241}Am is being produced in considerable amounts in nuclear reactors. It is an α-emitter with a half-life of 432 years and therefore

---
* SCK-CEN, Mol, Belgium

it shows a rather high specific activity. The main problem in measuring the fission cross section by fragment detection of ^{241}Am lies in the discrimination of about 10^7 to 10^8 α-particles against 1 fission event if one measures it in neutron fluxes available from electrostatic accelerators. The measurements were performed using the fast fission ionisation chamber with inherent discrimination against α-particles as described in a paper by C. Budtz-Jørgensen and H.-H. Knitter. The fission detector records in a back to back geometry the fission events from the ^{235}U and from ^{241}Am deposits at zero degree with respect to the incident ion beam of the accelerator. The total energy spread was ± 12 keV in the case where the neutrons were produced by the ^{7}Li(p,n)^{7}Be reaction at neutron energies below E_n = 1.2 MeV. In the neutron energy range from 1.2 to 4.5 MeV the T(p,n)^{3}He reaction was used to produce the neutrons. Here the total neutron energy spread varied between ± 50 and ± 75 keV. For the energies above 4.5 MeV the D(d,n)^{3}He reaction was used yielding a neutron energy spread of ± 100 keV for the few points we have measured until now.
At a distance of several meters from the neutron producing target we installed a neutron time-of-flight spectrometer to measure the neutron spectra. This allowed to make corrections due to some neutron contaminants in the spectrum as e.g. due to the second neutron group of the ^{7}Li(p,n)^{7}Be*-reaction. The measurements in the above mentioned energy range are completed, however, the ^{241}Am material has to be analysed for contaminants of non-threshold fissile material by mass-spectroscopic techniques.

<u>Test Measurements of the Neutron Induced ^{241}Am Fission Cross Section in the Energy Range 1 eV to 200 keV using the Linac</u>

C. Budtz-Jørgensen, H.-H. Knitter, J. Theobald*

The ionisation chamber with intrinsic suppression of alpha particle, loaded with 4 mg of ^{241}Am, was exposed to the neutron beam at 8 m distance from the Linac target. The resolution was between 1 and 8 nsec/m. The fission time-of-flight spectrum showed lines from ^{241}Am and also from ^{239}Pu. It was estimated that the sample material contains about 1% of ^{239}Pu. Therefore, a new chamber is constructed which will be loaded with a 30-40 mg ^{241}Am sample containing only ppm's of non-threshold fissile material. The measurements will be made relative to the ^{6}Li(n,α)T standard cross section.

---

* Technische Hochschule, Darmstadt, Germany

Fission widths of Subthreshold Fission Resonances of ^{241}Am

J. Theobald*)

The subthreshold fission cross section of $^{241}Am + n$, displayed in the EUR-report 4525e, have been analysed and compared to results obtained at Los Alamos (1) and Saclay (2). The following Table 2.2 gives the Γ_f values of resonances below 60 eV.

The average fission widths from the resonances compared are respectively:

$<\Gamma_f>_{Saclay} = 0.276$ meV; $<\Gamma_f>_{Geel} = 0.274$ meV;
$<\Gamma_f>_{L.A.S.L.} = 0.57$ meV.

The Los Alamos data taken with bombshot neutrons have been measured with fragments, the Saclay and Geel data with fission neutron detection techniques. Although the error on the Geel fission widths is about 25%, there remain considerable discrepancies between the results of the three laboratories, which call for new measurements.

REFERENCES

(1) P.A. SEEGER et al.
Nucl. Phys. A 96, 605, 1967

(2) H. DERRIEN, B. LUCAS
NBS Special publication 425, Vol. II, Proceedings of the conference "Nuclear Cross Sections and Technology" 1975, p. 637

*) Technische Hochschule, Darmstadt, Germany

TABLE **2.2**

E_0 (eV) Saclay(1975)	E_0 (eV) Geel(1969)	Γ_f (meV) Saclay(1975)	Γ_f (meV) Saclay(1975)*	Γ_f (meV) Geel(1969)
1.28	1.27	0.37		0.17**
1.93	1.94	0.08		0.09
2.37	2.39	0.18		0.10
2.60	2.59	0.17		0.11
3.97	3.99	0.16		0.08
4.97	4.98	0.44		0.10
5.42	5.42	0.63		0.13
6.12	6.13	0.42		0.14
9.12	9.12	0.18		0.04
9.85	9.87	0.95		0.24
10.40	10.44	0.06		0.06
10.99	10.95	0.13		0.21
12.88	12.87	0.06		0.05
14.68	14.70	0.27		0.14
15.69	15.80	0.10		0.17
16.39	16.43	0.11		0.13
16.86	16.86	0.32		0.17
17.73	17.70	0.30		0.25
(22.50)			0.58	1.62
24.19	24.19	0.14	0.48	0.17
25.63	25.56	0.29	0.82	0.27
31.25	31.31	0.22	0.57	0.84
36.98	36.93	0.51	0.66	0.33
38.37	38.40	0.30	0.53	0.35
39.62	39.96	0.23	0.56	0.47
50.21			0.37	0.58
57.25				0.38

* Obtained from evaluation of Saclay and Los Alamos data

** without selfscreening correction

3. STANDARD NEUTRON CROSS SECTION DATA AND RELATED INVESTIGATIONS

Cross Sections for the ^{6}Li+n System

H.-H.Knitter, C.Budtz-Jørgensen, M.Mailly, R.Vogt

The $^{6}Li(n,t)^{4}He$ cross section is one of the most important neutron cross section standards. An improvement of the knowledge of the ^{6}Li+n system in the neutron energy range from 0.1 to 5.0 MeV is desired.
The measurements were performed using the Van de Graaff accelerator of CBNM as a pulsed and monoenergetic neutron source. In the neutron total and differential elastic scattering cross section measurements the neutron detection was made by a neutron time-of-flight spectrometer system. The detectors were plastic scintillators mounted on fast photomultiplier tubes. The angular position of the detectors with respect to the direction of the neutrons incident on the ^{6}Li sample could be steered automatically. Details of the experimental set-up are described in [1].
The total and the integrated elastic scattering cross sections exhibit a large resonance, with the maximum of the total cross section appearing at $E_n=(247 \pm 3)$keV. This resonance is already known to be a $5/2^-$ resonance and this is also evident from the behaviour of the centre-of-mass Legendre coefficients.
From the elastic neutron scattering angular distribution it can be seen that below 1.5 MeV incident neutron energy only s- and p-wave neutrons are interacting since in this region the centre-of-mass Legendre coefficients B_L with $L > 2$ are zero. Interference of possible p-wave resonances at higher energies with the present resonance can only be very small since the B_2 coefficient approaches zero in the neutron energy region from 1 to 1.5 MeV. The known $5/2^-$ resonance below the neutron binding energy at an excitation energy of 6.64 MeV of the ^{7}Li nucleus has an extremely small reduced neutron width of $\gamma_n^2 = (0.00 \pm 0.01)$MeV as determined by Spiger and Tombrello [2]. It follows that all the transition probabilities will be negligibly small for processes containing this neutron channel. In addition this implies that the $5/2^-$ resonance below the neutron binding energy can not give a contribution to the (n,t) and (n,n) processes in the region of the 247 keV resonance. Due to the above mentioned reasons, a single isolated resonance is considered and for the representation of the total and the integrated elastic scattering cross section a single level Breit-Wigner formula plus linear background terms are used. These background terms account for the potential scattering and for an eventual contribution from distant levels. The $1/\sqrt{E}$ dependence of the (n,t) cross section [3] is also included. These terms lead to the equations for the neutron total and integrated elastic scattering cross section of ^{6}Li

$$\sigma_T(E) = a_1 + a_2E + \frac{0.14956}{\sqrt{E}} + \frac{\pi\lambda\!\!\!^{-2}(2J_\circ+1)}{(2i+1)(2I+1)} \cdot \frac{\Gamma_n^2 + \Gamma_n.\Gamma_\alpha}{(E_\circ+\Delta-E)^2+1/4(\Gamma_n+\Gamma_\alpha)^2} \quad (1)$$

$$\sigma_{n,n}(E) = a_3 + a_4E + \frac{\pi\lambda\!\!\!^{-2}(2J_\circ+1)}{(2i+1)(2I+1)} \cdot \frac{\Gamma_n^2}{(E_\circ+\Delta-E)^2+1/4(\Gamma_n+\Gamma_\alpha)^2} \quad (2)$$

with $\Gamma_n=2\gamma_n^2\, P_n(E)$ and $\Delta= -\gamma_n^2\, (S_n(E)-S_n(E_\circ))$; γ_n^2 is the reduced neutron width, $P_n(E)$ and $S_n(E)$ are the neutron penetration and shift function respectively.
In accordance with the fact that the Legendre coefficient with $L > 2$ are zero, only the neutron subchannel with a channel spin 3/2 and orbital angular momentum 1 was used. The used interaction radius was 3.89 fm. A simultaneous fit to the total and integrated elastic cross section was made using all the cross section data up to 1.5 MeV by minimizing

$$\chi^2=\sum_i\left(\frac{\sigma_T(E_i)_{exp.}-\sigma_T(E_i)_{cal}}{\Delta\,\sigma_T(E_i)_{exp.}}\right)^2+\sum_j\left(\frac{\sigma_{n,n}(E_j)_{exp.}-\sigma_{n,n}(E_j)_{cal}}{\Delta\,\sigma_{n,n}(E_j)_{exp.}}\right)^2 \quad (3)$$

This procedure allows a determination of the unknown parameters contained in equation (1) and (2). The following numerical results were obtained :

$a_1= (0.616 \pm 0.020)$b $\qquad a_2= (0.209 \pm 0.015)\text{b.MeV}^{-1}$
$a_3= (0.631 \pm 0.049)$b $\qquad a_4= (0.090 \pm 0.048)\text{b.MeV}^{-1}$

$\gamma_n^2= (1.082 \pm 0.017)$MeV $\qquad \Gamma_\alpha= (0.0357 \pm 0.0015)$MeV
$E_\circ= (0.2502 \pm 0.007)$MeV.

The curves obtained by the fitting procedure for the total cross section and for the integrated elastic scattering cross section are plotted as full lines in Fig. 3.1.
The shape of the total cross section peak as given by the experimental points is very well represented by the calculated curve. The maximum of the total cross section has a value of (11.27 ± 0.12)b and appears at the incident neutron energy of (247 ± 3)keV.
The B_2 centre-of-mass Legendre polynomial expansion coefficient of the elastic neutron scattering angular distribution can be calculated from the parameter obtained by the fit without additional assumption. By specifying the general formula for the Legendre coefficients to this specific case one obtains

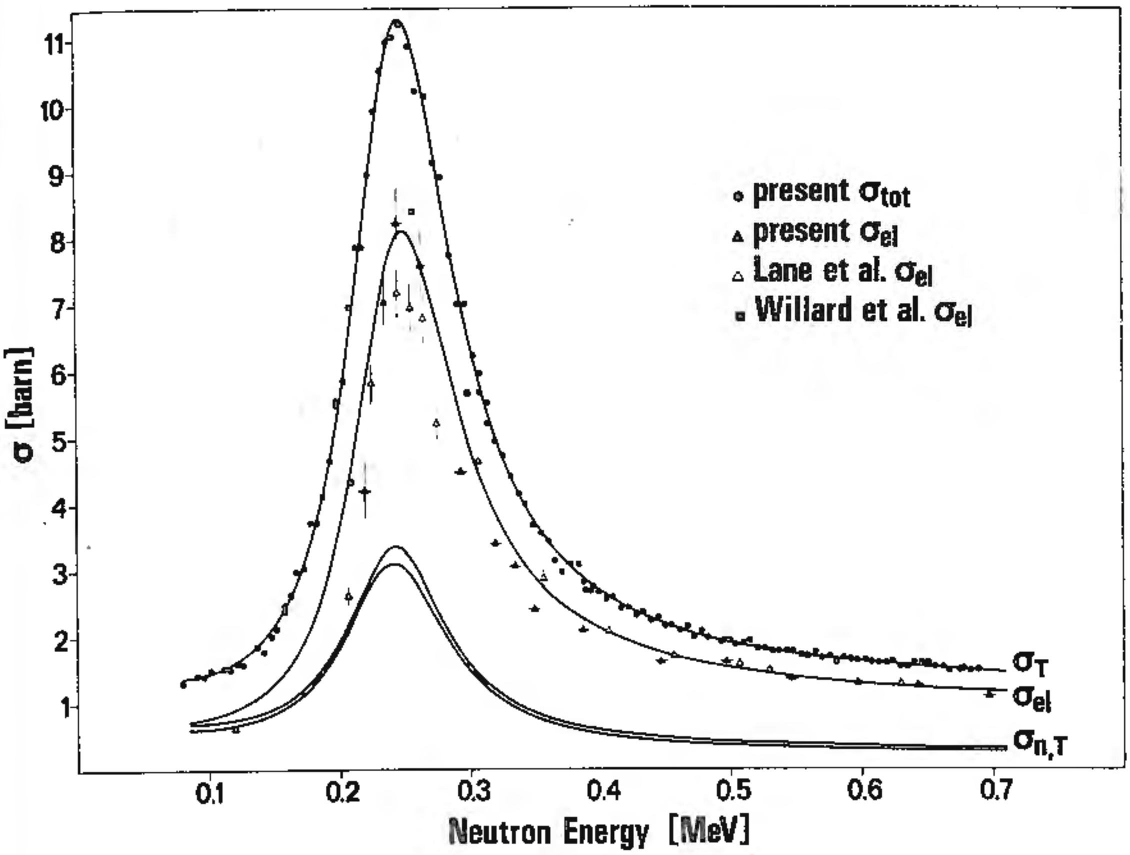

Fig. 3.1 The neutron total integrated elastic and (n,T) cross sections of ^{6}Li are plotted versus the incident neutron energy. Curves are obtained from the fit.

$$B_2(E) = \frac{ƛ^2}{(2i+1)(2I+1)} Z^2(I,J_o,1,J_o/s,2) \frac{(1/2\Gamma_n)^2}{(E_o+\Delta-E)^2+1/4(\Gamma_n+\Gamma_\alpha)^2} \tag{4}$$

The calculated values of the B_2 coefficient are plotted as the full line in Fig. 3.2. As can be seen, the agreement between the calculated and observed values of the B_2 coefficient is good. The B_1 coefficient cannot be calculated from the above parameters without additional assumptions about the potential scattering phase shift for the channel spin 3/2 and the orbital angular momentum zero. However, the information contained in B_1 could be used in a comprehensive R-matrix fit.
The ^{6}Li(n,t)^{4}He cross section was also calculated. The errors of the (n,t) cross section were obtained from error propagation calculations using the parameters and their errors as obtained from the least squares fit. The ^{6}Li(n,t)^{4}He cross sections and their errors are given in Table 3.1 for convenient neutron energy steps. Good agreement is found with the most

TABLE **3.1**

^{6}Li(n,t)^{4}He cross section from 0.08 to 0.50 MeV

SIG(b)	DSIG(b)	E(MeV)	SIG(b)	DSIG(b)	E(MeV)
0.657	0.042	0.085	1.658	0.044	0.295
0.656	0.042	0.090	1.531	0.040	0.300
0.658	0.042	0.095	1.417	0.037	0.305
0.663	0.041	0.10D	1.316	0.035	0.310
0.670	0.041	0.1D5	1.226	0.034	0.315
0.680	0.041	0.110	1.146	0.033	0.320
0.692	0.041	0.115	1.074	0.033	0.325
0.708	0.041	0.12D	1.011	0.032	0.330
0.727	0.041	0.125	0.954	0.032	0.335
0.749	0.041	0.130	0.903	0.031	0.340
0.775	0.041	0.135	0.857	0.031	0.345
0.806	0.041	0.140	0.815	0.031	0.350
0.842	0.042	0.145	0.778	0.030	0.355
0.884	0.042	0.150	0.744	0.030	0.360
0.932	0.042	0.155	0.713	0.030	0.365
0.988	0.043	0.160	0.686	0.030	0.370
1.053	0.044	0.165	0.660	0.029	0.375
1.128	0.044	0.170	0.637	0.029	0.380
1.214	0.045	0.175	0.615	0.029	0.385
1.313	0.046	0.180	0.595	0.029	0.390
1.427	0.047	0.185	0.577	0.028	0.395
1.557	0.048	0.190	0.560	0.028	0.400
1.704	0.048	0.195	0.545	0.028	0.405
1.870	0.048	0.200	0.530	0.028	0.410
2.052	0.047	0.205	0.517	0.028	0.415
2.250	0.048	0.210	0.504	0.027	0.420
2.456	0.051	0.215	0.493	0.027	0.425
2.663	0.058	0.220	0.482	0.027	0.430
2.858	0.071	0.225	0.472	0.027	0.435
3.024	0.088	0.230	0.462	0.026	0.440
3.147	0.105	0.235	0.453	0.026	0.445
3.211	0.119	0.240	0.445	0.026	0.450
3.212	0.129	0.245	0.437	0.026	0.455
3.149	0.131	0.250	0.429	0.026	0.460
3.033	0.126	0.255	0.422	0.025	0.465
2.876	0.116	0.260	0.416	0.025	0.470
2.695	0.103	0.265	0.410	0.025	0.475
2.504	0.090	0.270	0.404	0.025	0.480
2.312	0.077	0.275	0.398	0.025	0.485
2.128	0.066	0.280	0.393	0.024	0.490
1.957	0.056	0.285	0.388	0.024	0.495
1.800	0.049	0.290	0.383	0.024	0.500

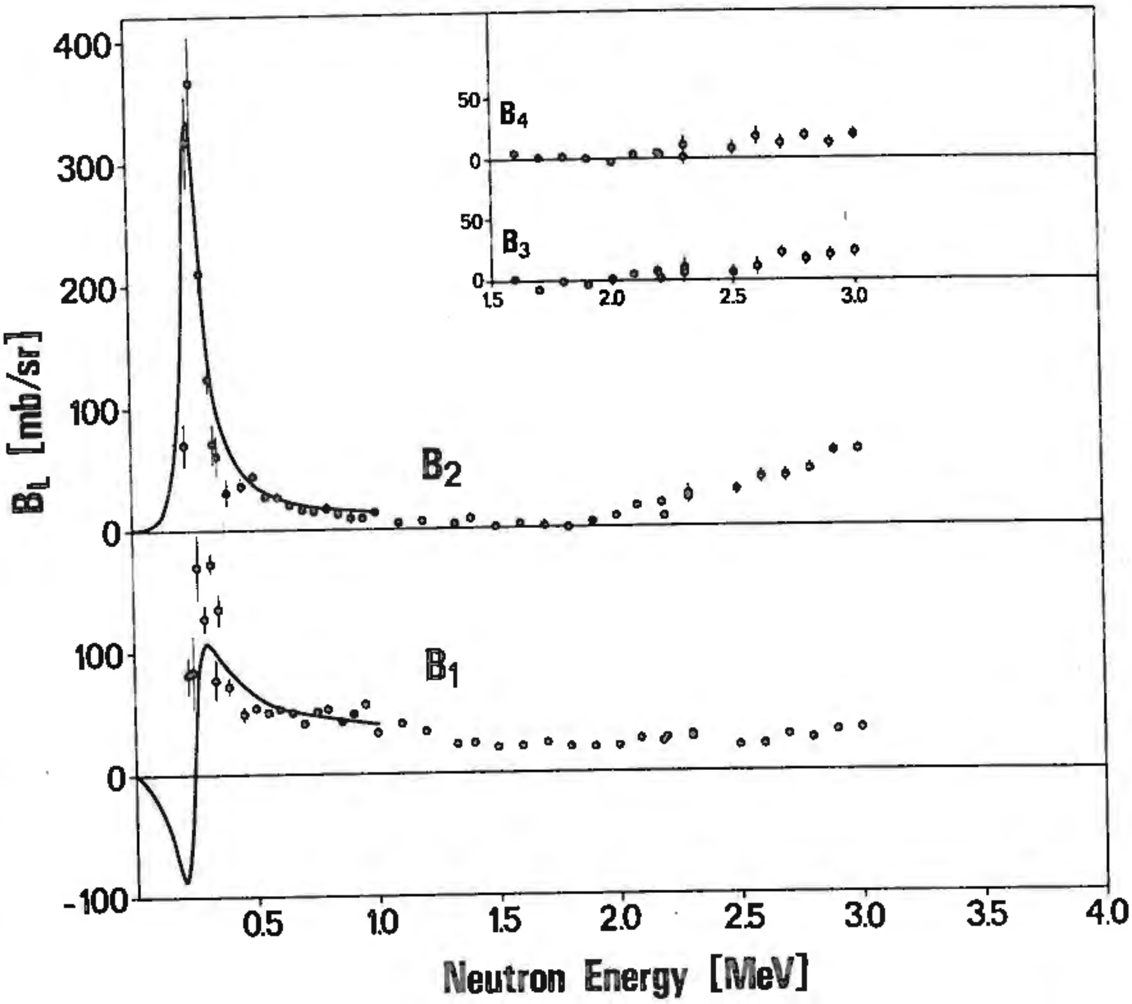

Fig. 3.2 Centre of mass legendre polynomial expansion coefficients of neutron elastic scattering angular distributions of ^{6}Li.
Solid lines are calculated curves.

recent direct measurements [4] [5] . There is however a large disagreement with the data of [6] . The detailed results of the present work are published in [1] .

<u>References</u>

[1] H.-H.KNITTER, C.BUDTZ-JØRGENSEN, M.MAILLY, R.VOGT, Report EUR-5726e (1977).

[2] R.J.SPIGER, T.A. TOMBRELLO Phys. Rev., <u>163</u>, 964, (1967).

[3] L.STEWART,
Proc. of "Neutron Standard Reference Data", IAEA Panel Proc. Series, 149, VIENNA,(1972).

[4] G.P. LAMAZE, O.A.WASSON, R.A. SCHRACK, A.D. CARLSON,
Intern. Conf. on the Interactions of Neutrons with Nuclei, Lowell, Massachussetts, 6-9 July, 1976, Vol.2, p. 341.

[5] D.B.GAYTHER,
AERE-8556,(1977).

[6] S.J.FRIESENHAHN, V.J.ORPHAN,A.D.CARLSON, M.P.FRICKE,W.M.LOPEZ,
Report INTEL-RT 7011-001, (1974).

Survey of recent Experiments for the ^{7}Li-System

H.-H.Knitter

As an invited paper for the International Specialists Symposium on Neutron Standards and Applications held in Gaythersburg (USA) in 1977, a survey of recent experiments for the ^{7}Li-system was elaborated [1]. Experiments on reactions relevant to the ^{7}Li-system are described. It concerns the reactions ^{6}Li(n,t)^{4}He, ^{6}Li(n,n)^{6}Li, ^{4}He(t,n)^{6}Li and ^{4}He(t,t)^{4}He, for which differential cross sections $\sigma_i(E,\Theta)$, angle integrated cross sections $\sigma_i(E)$ and neutron total cross sections $\sigma_T(E)$ were measured. Also polarization experiments yielding the analyzing power $A_i(E,\Theta)$ are described.

References

[1] H.-H.KNITTER,
Survey of recent experiments for the ^{7}Li-system, NBS Special Publication 493, page 3, (1977), Proceedings of a Symposium on Neutron Standards and Applications.

Review of Cross Section Measurements for the ^{10}B+n System

E.Wattecamps

Detectors relying on the ^{10}B(n,α)^{7}Li reaction are widely used for the flux determination of thermal, epithermal or fast neutrons. The cross section underlying the neutron flux determination is $\sigma(n,\alpha)$ with $\sigma(n,\alpha) = \sigma(n,\alpha_0) + \sigma(n,\alpha_1)$. The α_0 refers to the emission of an α particle of about 1.8 MeV for a neutron interaction at thermal energy, leaving the ^{7}Li nucleus in its ground state. The α_1 refers to the emission of an α particle of about 1.5 MeV for a neutron interaction at thermal energy, leaving the residual nucleus in its first excited state, which decays by prompt 478 keV gamma ray emission. Some detectors rely on the detection of this gamma ray, and therefore $\sigma(n,\alpha_1)$ data are requested as well as $\sigma(n,\alpha)$ data.

Therefore, the CBNM has undertaken an effort to compile cross section data of the $^{10}B(n,\alpha)^7Li$ and of the $^{10}B(n,\alpha_1)^7Li^*$ reaction together with related cross section data such as $\sigma(n,\alpha_o)$, σ_{tot}, $\sigma_{n,p}$, branching ratio and the ratio of $\sigma(n,\alpha)$ of ^6Li to ^{10}B.

This compilation, together with some qualitative arguments on accuracies is part of CBNM's contribution to the INDC and NEANDC meetings on standards and discrepancies.

The compilation deals with about 5000 pairs of energy and cross section values. Most of the data have been obtained on magnetic tape from the CCDN, Centre de Compilation de Données Neutroniques, Paris; some data were taken from publications and in some very few cases numerical data have been extracted from published graphs. All data were put on cards in the same format in a single set of units (eV, barn). Some data sets with high resolution but poor statistical accuracy were summed into groups with improved statistical accuracy. Plots were made at the CBNM computer with the code ANGELA. The scale of the plots was adapted individually to get a clear picture even if a drawing comprises thousand data points. Together with the experimental data a continuous curve is drawn which is the ENDF/B-IV evaluated data.

As an example, Fig. 3.3 shows cross section data for σ_{tot}, $\sigma(n,\alpha_o) + \sigma(n,\alpha_1)$, $\sigma(n,\alpha_1)$ and $\sigma(n,\alpha_o)$ between 100 eV and 20 MeV neutron energy.

An investigation of assessable accuracies of fits on the basis of a quantitative analysis is in progress now for some selected cross section types and began with the compilation of an error file.

The compilation of $\sigma(n,\alpha)$ and $\sigma(n,\alpha_1)$ cross section data shows that data requests from 10 keV to 1 MeV are not fulfilled. To define recommendable data with assessable accuracies a new evaluation is recommended. The evaluation ought to take full accounts of, and be consistent with, related and available accurate cross section data, such as branching ratios and $\sigma(n,\alpha)$ ratios of ^6Li and ^{10}B.

It is questionable whether new measurements of σ_{tot} from 400 keV to 1 MeV would reduce the error margins of $\sigma(n,\alpha)$.

New measurements of $\sigma(n,\alpha_1)$ or $\sigma(n,\alpha)$ are inevitable if one has to achieve 2 % accuracy up to 1 MeV. The large scattering of present $\sigma(n,\alpha)$ data and the common use of $\sigma(n,\alpha_1)$ for flux determination in cross section measurements tend to recommend primarily new $\sigma(n,\alpha_1)$ and branching ratio measurements.

Cross section ratio measurements above 10 keV of $\sigma(n,\alpha)$ of ^6Li to ^{10}B with a single detector are recommended. Evaluations of ^{10}B and ^6Li cross section data should yield data sets which are consistent with the measured ratio of $\sigma(n,\alpha)$ of

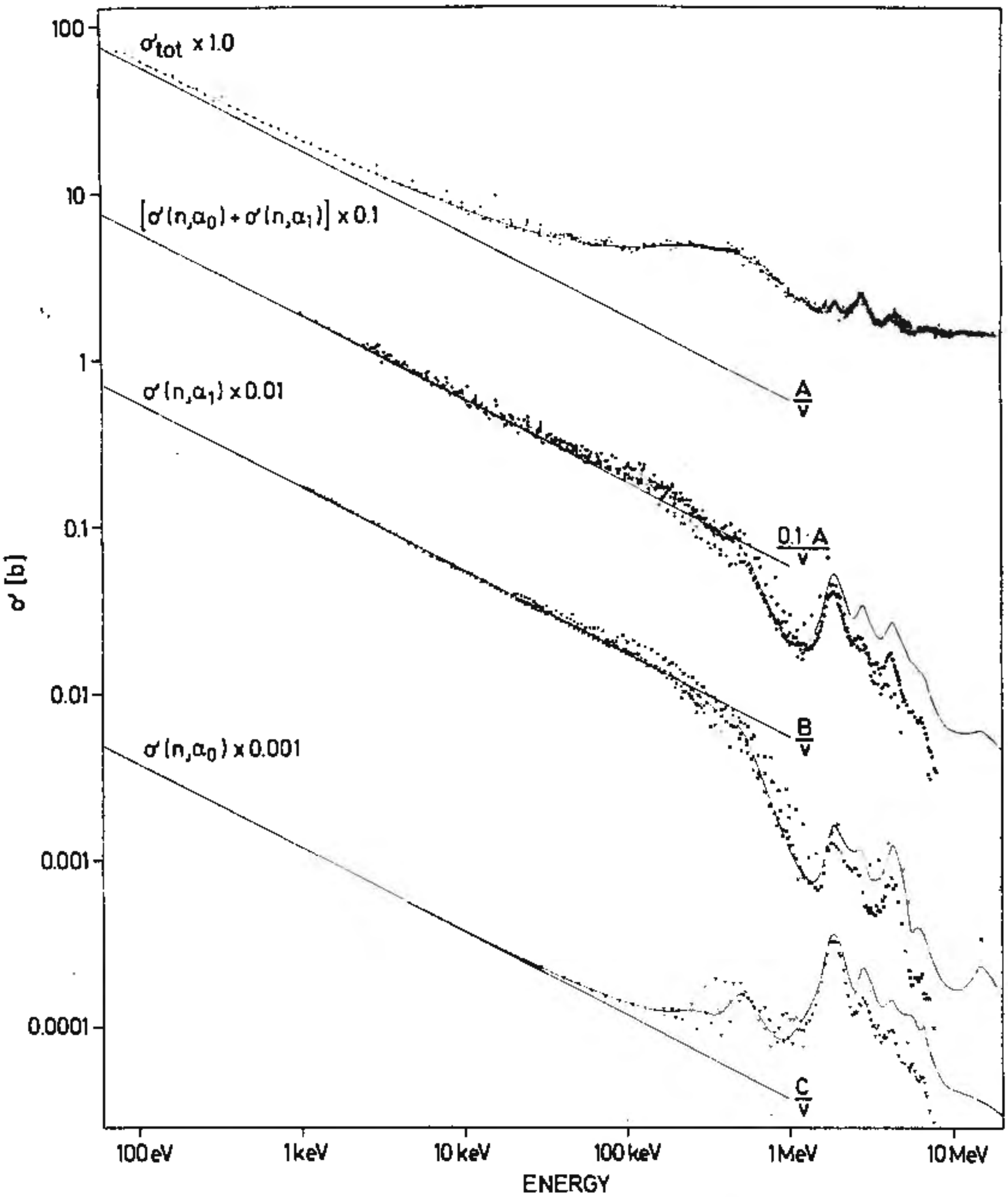

Fig. 3.3 Cross-sections: σ_{tot}, $\sigma(n,\alpha_0)+\sigma(n,\alpha_1)$, $\sigma(n,\alpha_1)$ and $\sigma(n,\alpha_0)$. Continuous curves are ENDF/B IV 1975 evaluation.

^{6}Li to ^{10}B.

Best Values for the Cross Section of the Neutron Standard Reaction $^{10}B(n,\alpha_1)^7Li^*$ in the 0.1 to 2.0 MeV Range

H.Liskien, E.Wattecamps

The boron slab detector in which the 478 keV gamma ray is observed from the $^{10}B(n,\alpha_1)^7Li^*$ reaction, is a fast device often applied in neutron time-of-flight experiments. Therefore the $^{10}B(n,\alpha_1)$ cross section has been included in the system of neutron cross section standards [1]. Typically the γ-detection geometry is complicated and the intrinsic photopeak efficiency is unknown. Therefore the boron slab detector is mostly applied to determine the flux only in relative units, this means results are obtained only part from an unknown, but neutron energy independent constant. Consequently also the $^{10}B(n,\alpha_1)$ cross section has not to be known on an absolute scale, but its energy dependence is sufficient. Recently [2], all the available experimental information on the $^{10}B(n,\alpha_1)$ reaction has been compiled. Below 100 keV all data except those of Friesenhahn et al. show reasonable agreement and it seems likely that the accuracy of evaluated data may reach the $\pm$ 2 % level. The present evaluation covers the range from 100 keV to 2 MeV and aims at best values on a smooth curve. Within the energy region under consideration 44 energies were chosen. From the experimental data as compiled in ref. 2, cross sections at these energies were derived. The various sets have been combined by multiplying each by a normalization factor and finding best values for these factors so that

a) the relative deviation from the mean (summed for all sets and groups) becomes a minimum, and
b) the best value for the cross section at 100 keV agrees with the ENDF/B-IV value (1.82 b).

We have given equal weights to the individual cross sections for the following reasons : firstly, because the existing discrepancies indicate that total uncertainties have been underestimated in nearly all cases and secondly, because the partial uncertainties related only to the shape could not be deduced from the published information. Certain data were excluded. The resulting renormalized cross sections are given in Table 3.2 together with the normalization factors found. The standard deviation $\Delta\sigma_i$ for all values belonging to a set i was calculated according to

$$\Delta\sigma_i = \sqrt{\frac{1}{(n_i-1)} \cdot \sum_j \left(1-\frac{\sigma_{ij}}{\langle\sigma_j\rangle}\right)^2} \quad .$$

$\langle\sigma_{ij}\rangle$ is the renormalized cross section from set i at energy indexed j,
σ_j is the mean value of all renormalized cross section at energy indexed j.
For the summation over the energy index j only those n_i values were taken into account for which also other sets, beside i, has contributed. Results are given in Table 3.2 and Figure 3.4 , where $\sigma\cdot\sqrt{E}$ (b.MeV$^{1/2}$) is plotted versus E (MeV) on lin/log scales.

A smooth eye-guide cruve through the average of the normalized cross sections

TABLE 3.2

RENORMALIZED CROSS SECTIONS, CERTAIN DATA EXCLUDED

NORMALIZ.-FACTOR		DAVIS 1.041	MACKLIN 1.114	COATES 1.056	FRIESENHAHN 0.822	SEALOCK 1.034	SCHRACK 1.004	MEAN
NR	EN(MEV)	SIGMA(B)	SIGMA(B)	SIGMA(B)	SIGMA(B)	SIGMA(B)	SIGMA(B)	SIGMA(B)
1	0.100		1.974	1.856	1.727		1.841	1.849
2	0.110			1.764	1.694		1.759	1.739
3	0.120			1.684	1.607			1.645
4	0.130			1.603	1.574		1.577	1.584
5	0.140			1.565	1.523			1.539
6	0.150			1.512			1.461	1.487
7	0.160			1.455	1.405			1.430
8	0.170		1.473	1.387	1.362		1.388	1.403
9	0.180			1.309	1.271			1.290
10	0.190			1.290	1.253		1.317	1.287
11	0.200			1.235	1.233	1.128	1.262	1.214
12	0.220		1.163	1.151	1.128		1.185	1.157
13	0.240			1.059	1.047	1.009		1.038
14	0.260		1.007	0.963	1.011		1.036	1.004
15	0.280			0.902	0.931		0.972	0.935
16	0.300			0.815	0.870	0.878	0.939	0.876
17	0.325				0.809			0.809
18	0.350		0.726		0.751	0.817	0.790	0.771
19	0.375				0.685		0.747	0.716
20	0.400						0.700	0.700
21	0.425				0.672		0.662	0.667
22	0.450				0.613	0.661		0.637
23	0.475				0.601		0.621	0.611
24	0.500		0.516			0.596	0.578	0.563
25	0.550	0.515			0.505	0.455	0.474	0.487
26	0.600	0.401			0.412	0.360	0.374	0.387
27	0.650	0.334			0.335	0.332	0.280	0.320
28	0.700	0.268			0.276	0.266		0.270
29	0.750	0.232				0.219		0.225
30	0.800				0.226	0.198		0.212
31	0.850	0.182			0.182	0.185		0.183
32	0.900	0.148				0.158		0.153
33	0.950	0.142				0.155		0.148
34	1.000	0.135			0.146	0.126		0.135
35	1.100	0.090				0.106		0.098
36	1.200	0.085				0.087		0.086
37	1.300	0.078						0.078
38	1.400	0.073						0.073
39	1.500	0.070						0.070
40	1.600	0.087						0.087
41	1.700	0.125						0.125
42	1.800	0.132						0.132
43	1.900	0.127						0.127
44	2.000	0.120						0.120
STAND.	DEVIATION	4.0%	5.9%	2.6%	3.4%	5.1%	4.2%	

in the 0.10 to 0.25 MeV and 0.9 to 2 MeV region yields the recommended cross sections. In the 0.25 to 0.90 MeV region a straight line has been assumed to be the "background" below the $5/2^-$ resonance in ^{11}B. The differences between the average cross sections and this "background" have been fitted to

$$\Delta\sigma(E) = \frac{\sigma_o(\Gamma/2)^2}{(E-E_o)^2 + (\Gamma/2)^2} .$$

With an assumed uncertainty for $\Delta\sigma(E)$ of 0.01 b.MeV$^{1/2}$ for all differences a χ^2 of 0.7 is obtained. Our results are :σ_o=(140 $\pm$ 7)mb, Γ= (202 $\pm$ 7)keV, E_o= (468 $\pm$ 6)keV.

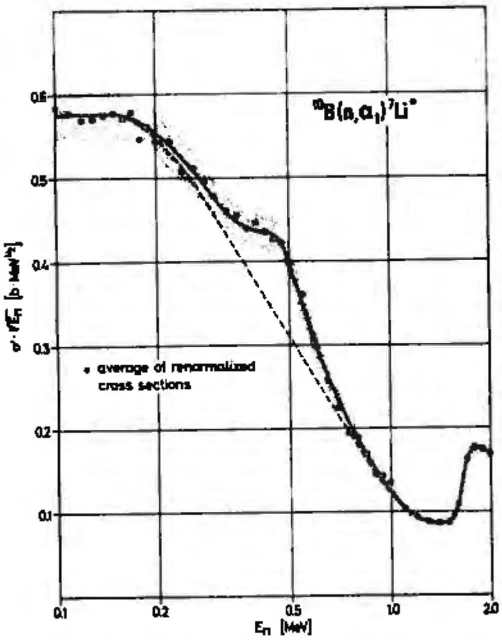

Fig. 3.4

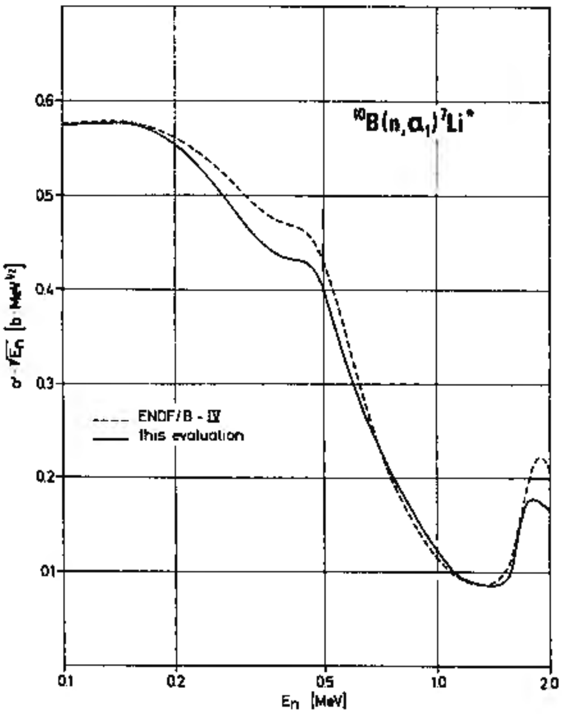

Fig. 3.5

The uncertainties have only restricted values as they do not include the influence from the assumption on the "background".
The suggested best curve is given in Figure 3.4 together with an arbitrarily chosen ± 5% uncertainty band. In Figure 3.5 comparison is made with the last issue of the ENDF/B standard file.
The present evaluation confirms the validity of the 1/v-law in the 0.1 to 0.15 MeV range within the experimental uncertainties and demonstrates the need for more accurate experimental cross section determination at higher energies. Such experiments are in progress at CBNM.

REFERENCES

[1] H. LISKIEN
Proc. of Intern. Conf. on the Interactions of Neutrons with Nuclei, Lowell (1976) Vol.II, p. 1110 - CONF-760715-P2.

[2] E. WATTECAMPS
Proc. of Intern. Specialists Symp. on Neutron Standards and Applications, Gaithersburg (1977), NBS Special Publication, 493, p. 67.

Determination of Relative Cross Sections for the Neutron Standard Reaction $^{10}B(n,\alpha_1)^7Li^*$ in the 0.1 to 2.2 MeV Range

G. Viesti, H. Liskien

Independent of the energy of a detected neutron, a "boron-slab" detector sees the same γ radiation (478 keV). Its intensity is proportional to the $^{10}B(n,\alpha\gamma)^7Li$

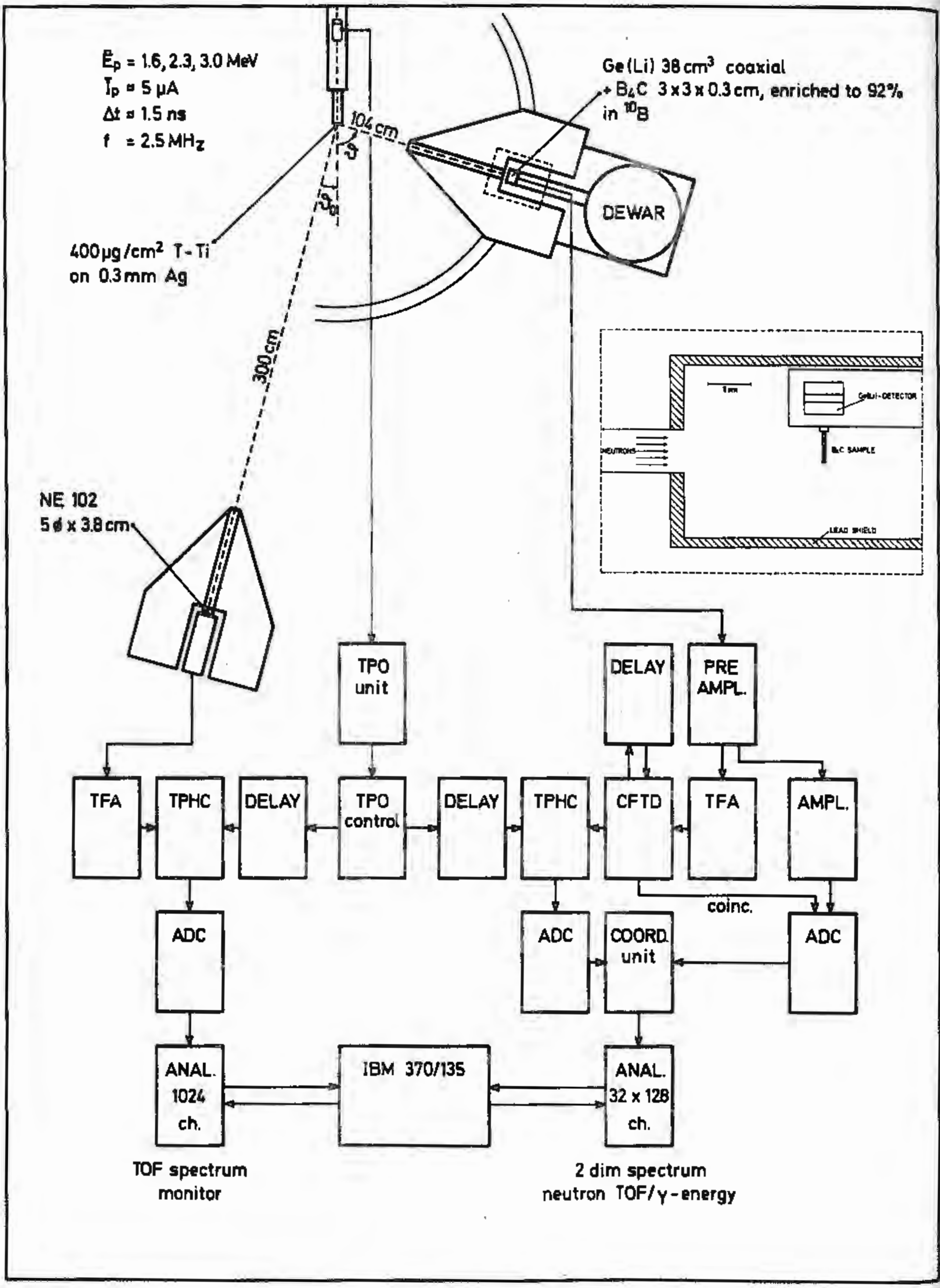

Fig. 3.6 Experimental arrangement for the measurement of the $^{10}B(n,\alpha\gamma)^{7}Li$ cross section.

cross section which is known above 100 keV neutron energy with insufficient accuracy. Using a B_4C-Ge(Li) system measurements are in preparation relative to the known angular distributions of the source reactions $^7Li(p,n)$ and T(p,n).
The geometrical and electronic set-up of the experiment is shown in Fig. 3.6.
A pulsed neutron source is obtained by bombarding a 400 $\mu g/cm^2$ T-Ti target with a 5 μA proton beam of the pulsed Van de Graaff of CBNM at proton energies of 1.6, 2.3 and 3.0 MeV. Using the angular range from 150 to 0° this corresponds to the overlapping neutron energy ranges of 0.1 to 0.7 MeV, of 0.3 to 1.4 MeV, and of 0.5 to 2.2 MeV respectively. The source strength is monitored by a TOF detector and the measurements performed relative to the well-known T(p,n) neutron angular distributions. A collimator is used to shield the 38 cm^3 coaxial Ge(Li)-detector which observes a 3 mm thick boroncarbide slab. For each event γ-pulse height and neutron time-of-flight are determined and stored in a two-dimensional memory. Special care has been taken to minimize neutron scattering into the Ge(Li)-detector, to shield the detector against γ's not stemming from the boron slab, and to optimize the timing resolution. Data at E_p = 1.6 and 2.3 MeV are taken and data analysis is in progress. Monte Carlo calculations for the determination of the attenuation and (multiple) scattering correction factor are in progress and this correction factor will be tested at E_p = 3.0 MeV with two B_4C slabs on different thickness.

Cross Section Fluctuations of Standard Reactions

H. Liskien, H. Weigmann

This work has been performed in order to assess cross section fluctuations due to level statistics. Such fluctuations prevent the successful application of a cross section standard for flux determinations when high resolution data are taken.
As basis of future discussion we have performed Monte-Carlo calculations to simulate the fluctuation of average cross section for the two standard reactions $^{197}Au(n,\gamma)$ and $^{235}U(n,f)$. For each compound spin, resonances are samples with level distances following a Wigner distribution and reduced level widths following a Porter-Thomas distribution. The contribution of each level is then calculated according to the single level Breit-Wigner expression. The average capture width was taken as constant. In the case of ^{235}U however, it has been increased artificially to 70, 100 and 160 meV at 100, 200, and 500 keV neutron energy, respectively, to roughly account for (n,n') deexcitation.
Fig. 3.7 shows the result, namely as function of the neutron energy the width of the neutron energy interval necessary to keep cross section fluctuations at 1, 3, 5 and 7%. It has to be stressed that the effect of additional intermediate structure has been ignored.
The results are published in Annals of Nuclear Energy 4 (1977) 38.

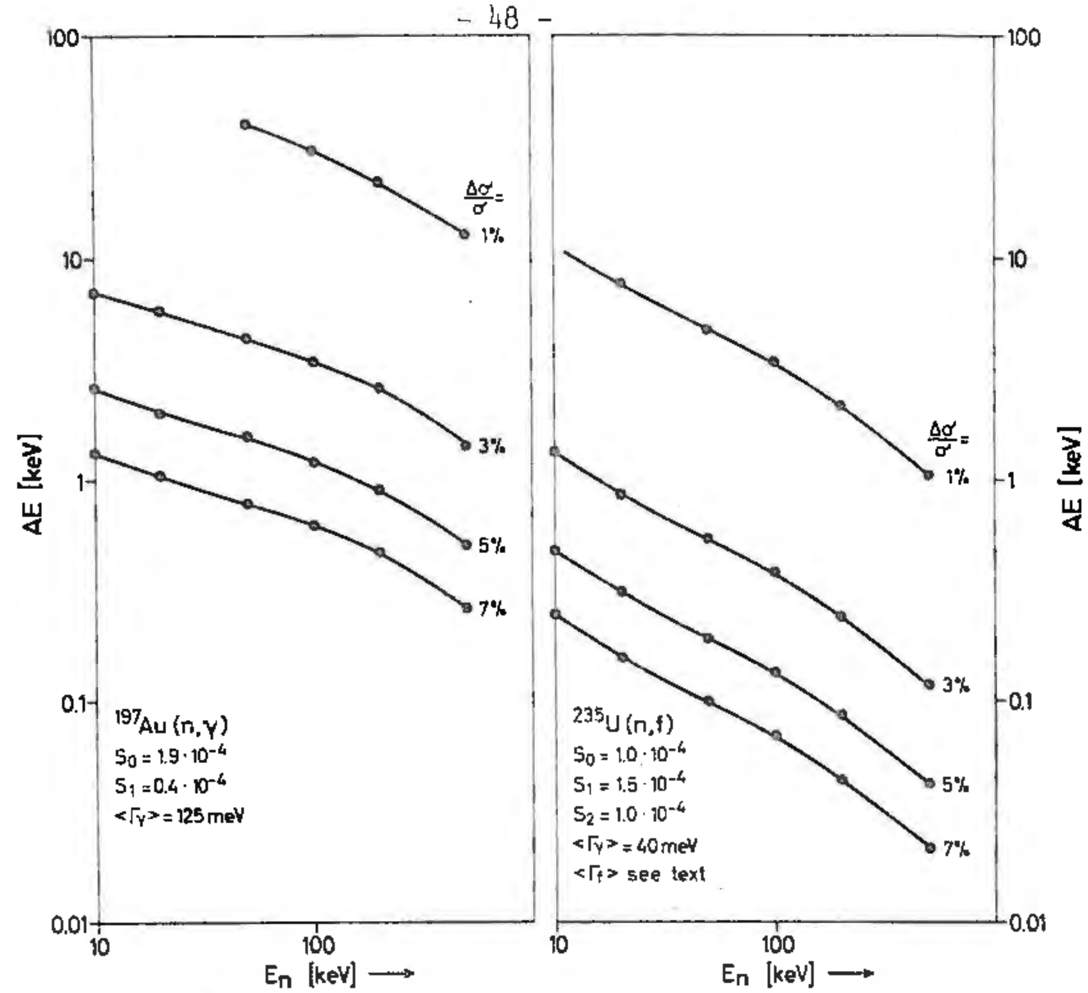

Fig. 3.7 Width of neutron energy interval ΔE necessary to produce a relative cross section fluctuation $\Delta\sigma'/\sigma'$ for the neutron energy range E_n from 10 to 500 keV.

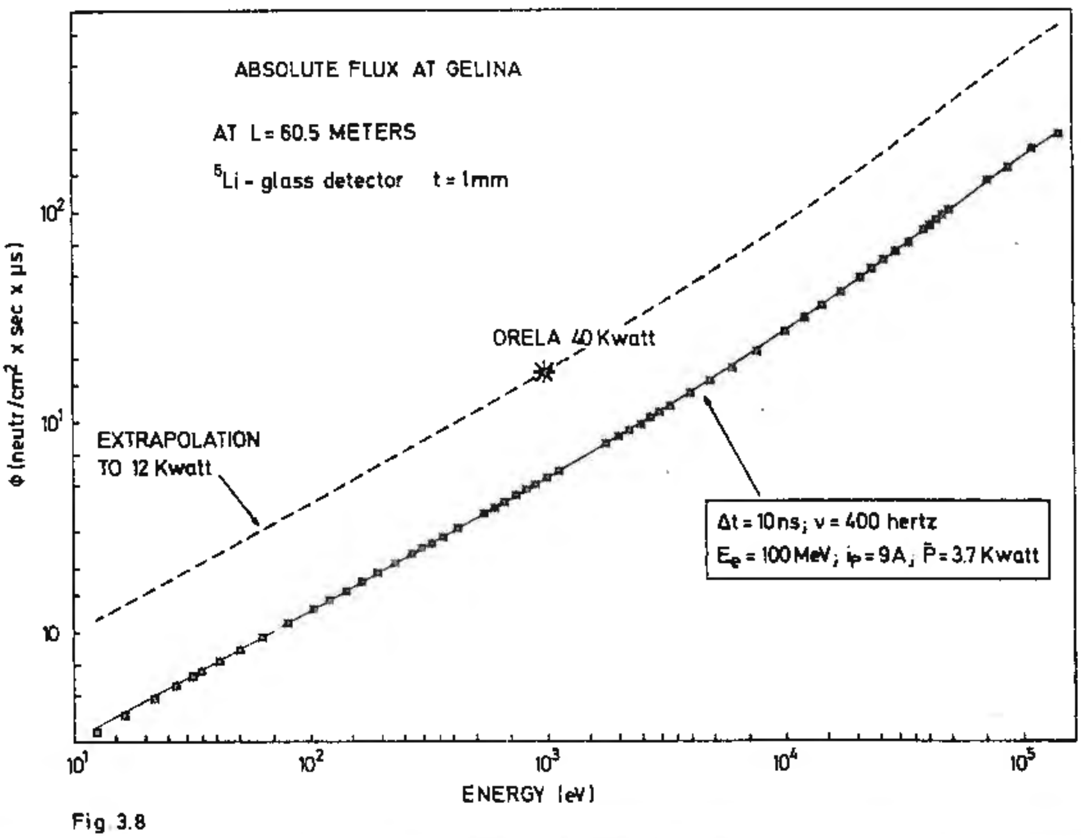

Fig 3.8

Neutron Flux Measurements at GELINA

G. Pasquariello, F. Corvi, T. van der Veen

In conjunction with the beginning of operation of the upgraded linac in March 1977, a programme of measurements of neutron flux was started, serving two main objectives:

a) accurate knowledge of the shape of the neutron flux from thermal up to a few hundred keV, necessary for the analysis of any partial neutron cross section measurements;
b) knowledge of the absolute neutron flux, useful for the design of new experiments and for comparisons with other machines and/or with calculations.

Two detectors were used:

a) sintered B_4C slab 3 mm thick enriched to 91% ^{10}B and viewed by two C_6D_6 liquid scintillators;
b) a 1 mm thick Li-glass scintillator type NE 912 enriched to 95% ^6Li.

By substracting the background, ranging from 1 to 5%, and correcting for variation of detector efficiency with energy, including multiple scattering effects, the raw data were transformed in a quantity proportional to the neutron flux $\phi(t)$, expressed in terms of neutrons per cm^2, per sec. and per nsec time-of-flight interval. Such a quantity was then fitted by a function of the type $\phi(E) = KE^{\alpha(E)}$ where E is the neutron energy in eV. One such fit is shown in Fig. 3.8 by a continuous line for Li-glass detector and a flight distance of 60.5 m.
The parameters of $\phi(t)$ are:

$$K = 0.0769$$

$$\alpha(E) = 0.603 + 0.381 \times 10^{-3}\sqrt{E} - 0.497 \times 10^{-6} E$$

The linac parameters related to the measurement are also given in Fig. 3.8.
By assuming proportionality between neutron flux and average beam power $\bar{P}$, one can extrapolate the results to the maximum power of 12 kW (see dotted line).
This should be compared with a value for ORELA at 40 kW which was deduced from a figure of 42.8 neutr./cm^2 x sec > eV at 1 keV and at 10 meter distance, given by Chrien.

This comparison shows that, at the guaranteed power of 12 kW, the Geel Linac delivers the same neutron flux as ORELA at 40 kW. This is equivalent to say that, at the same power, the "Geel U + moderator" assembly produces a factor of 3.3 more neutrons than the "ORELA Ta + water" source. The general expression for the neutron flux $\phi(E)$, in the range 7 eV - 140 keV for the Geel Linac as a function of average power and flight path distance is then :

$$\phi(E) = 1.67 \cdot 10^5 \cdot \frac{1}{E^{1.5-\alpha(E)}} \cdot \frac{P}{L^2} \text{ neutr./cm}^2 \cdot \text{sec} \cdot \text{eV}$$

where E is in eV, P is the power in kWatt and L is the flight distance in meters.

- oOo -

4. NON-NEUTRON NUCLEAR DATA

Studies on the Decay of $^{93}Nb^{m}$

W. Bambynek, G. Grosse, W. Oldenhof, D. Reher, R. Vaninbroukx

The study to get pure, carrier-free $^{93}Nb^{m}$ has been continued. There are two ways which were followed. One way is milking of $^{93}Nb^{m}$ from ^{93}Mo which could be produced by the reaction $^{93}Nb(p,n)^{93}Mo$ in a small cyclotron with sufficient beam current. The threshold energy and the cross-section for this reaction are E_{th} = 1.2 MeV and σ = 100 mb at a proton energy above the threshold of $E_p - E_{th}$ = 5 MeV [1]. With a beam of 30 μA and an irradiation time of two month about 10 μCi of ^{93}Mo could be produced. Discussions with laboratories having available such a cyclotron are going on. The second way is to separate ^{93}Zr from a high-level fission fragment solution which could be made available free of charge. One liter of such a solution, which has an activity of about 300 Ci, contains approximately 0.5 g ^{93}Zr. This corresponds to an activity of about 1 mCi. The $^{93}Nb^{m}$ could be milked from the ^{93}Zr solution. However, at CBNM no hot cells are available to work with such high activities. Discussions are going on with the Physikalisch-Technische Bundesanstalt (PTB) at Braunschweig, which is interested to cooperate in this project, and with some other laboratories having available suitable hot cells. In the meantime measurements have been performed with the source material available at CBNM. The measurements for the determination of the half-life of $^{93}Nb^{m}$ have been continued using Si(Li) detectors. Four sources prepared from two samples of different origin have been measured six times over a period of eight months. During this period only 3 % of the $^{93}Nb^{m}$ decayed. Consequently, the uncertainty is still of the order of 20 %. The mean value of the preliminary result is $T_{1/2}$ = (13.5 ± 2.5) years, which is definitely lower than the value of $T_{1/2}$ = (16.4 ± 0.4) years published recently by R. Lloret [2].

For the further decay studies the radioactive concentration of a master solution was determined using the liquid scintillation technique.

Fig. 4.1. shows an experimental energy spectrum. Integration and extrapolation to energy zero yield the disintegration rate of the sample.

From the peak position relative to the one photoelectron peak one can deduce that the mean number of photoelectrons hitting the first dynode of the photomultiplier is about 7. Assuming that the distribution of these photoelectrons is a Poissonian $P_n(m)$, where m is the mean number per event, the probability that n electrons hit the first dynode is $P_n(m)=\frac{m^n}{n!}\,e^{-m}$. The zero probability is $P_o=0.001$ and consequently the efficiency attainable by extrapolation to zero energy is 99.9%. Four sources were prepared quantitatively from the same solution and each measured three times during a period of two weeks. The random uncertainty of the main result of the 12 measurements is ± 0.4 % on a 99.7 % confidence limit, the linear sum of the systematic uncertainties is $\pm$ 0.2 %. The transition of $^{93}Nb^m$ to the ground state is highly converted. A search for a possible γ emission has been performed with the Compton-suppression spectrometer.

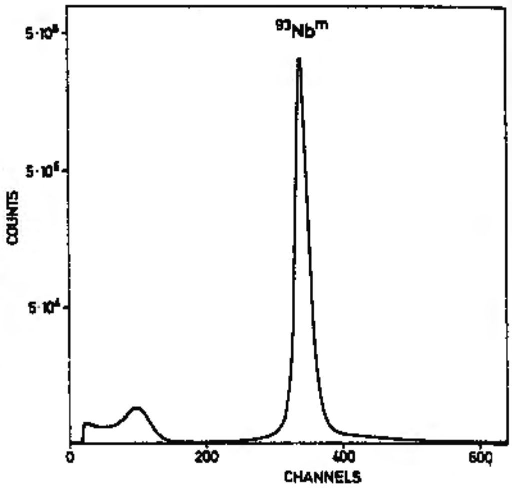

Fig. 4.1 Measurement of the disintegration rate of a $^{93}Nb^m$ solution with the liquid scintillation technique.

The γ line can clearly be identified, if the Compton background is suppressed. Preliminary values for the γ-ray energy and intensity are:

E_γ = (30.75 $\pm$ 0.10)keV and

I_γ = (4.5 $\pm$ 1.0)10^{-6}.

The improvement in the knowledge of the transition energy allows to make more accurate interpolations of tabulated theoretical internal conversion data as those of Hager and Seltzer [12] .

The KX-ray emission rate of three sources prepared quantitatively from the same solution as above was measured using calibrated Si(Li) detectors. Some corrections as for self-absorption of the KX rays and for Nb KX rays produced in the source material by interaction of the γ rays and β particles of impurities such as ^{94}Nb have still to be investigated. Preliminary results of these measurements are:

I_{KX} = 0.116 $\pm$ 0.004 and $I_{K\beta}/I_{K\alpha}$ = 0.189 $\pm$ 0.003.

The ratio of the K and L conversion electrons was measured with a 4 π proportional counter filled with an argon-methan mixture (9 : 1) at various pressures between 1 and 60 bar. Seven sources were prepared by drop evaporation with and without seeding agents (Catanac) and by electrospraying. A representative spectrum of the conversion electrons, which was measured with the source showing the smallest self-absorption is shown in Fig. 4.2.

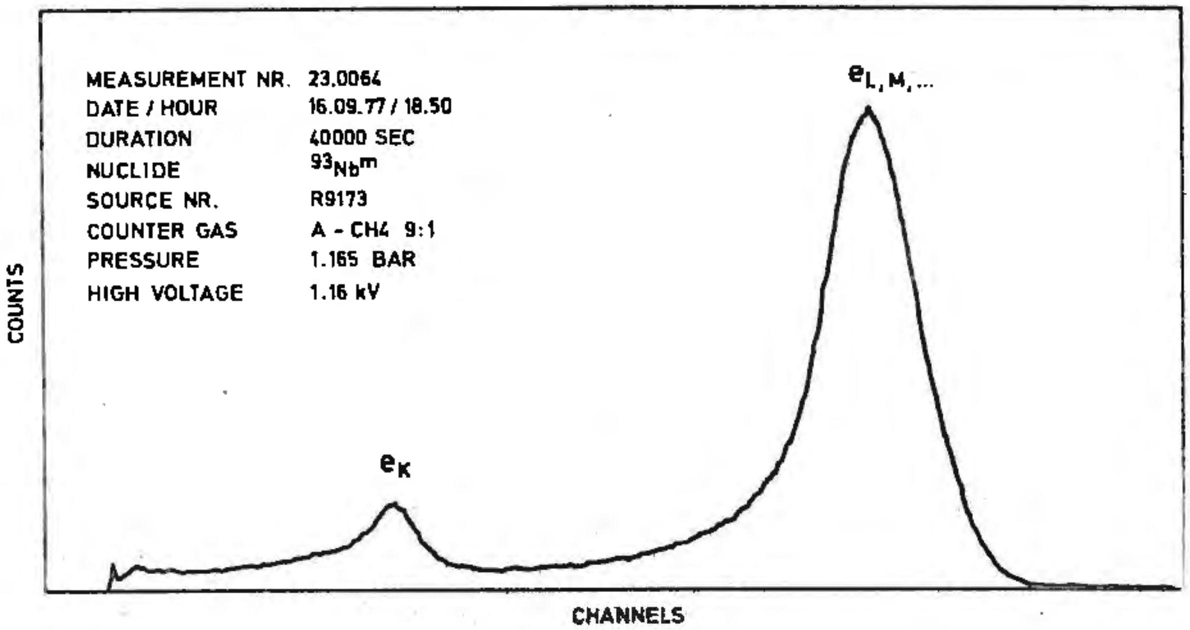

Fig. 4.2 Spectrum of the K and LM+... conversion electrons of $^{93}Nb^m$ measured with a proportional counter.

Corrections have been allowed for background, the influence of the KX rays, sum effects of the K Auger electrons and the K conversion electrons, and the separation of the peaks which introduced the greatest uncertainty. The separation of the K and the LM+.. peak from each other was done by fitting their low energy tails to an exponential function and extrapolation to zero energy (Fig. 4.3.).

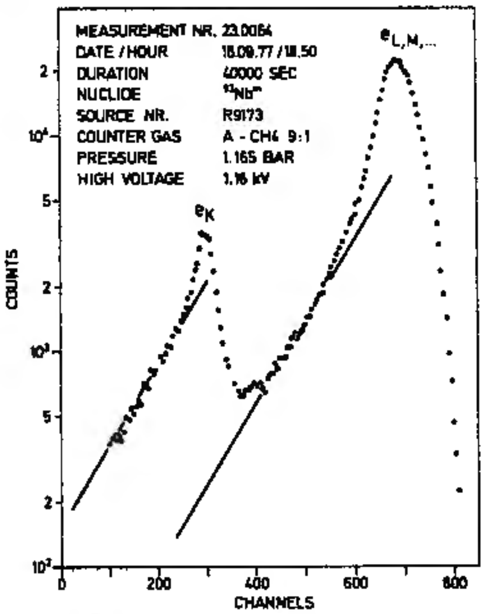

Fig. 4.3 The conversion electron spectrum of $^{93}Nb^m$ plotted in semi-log scale to correct for degradation in the low-energy tail

This is based on the assumption that the energy loss is of the same magnitude for both energies. A preliminary result deduced from these measurements is K/LM+ = 0.16 ± 0.03. From this value combined with the fluorescence yield ω_K(Nb) = 0.75 ± 0.03 [3] the KX-ray intensity can be calculated. The decuded value I_{KX} = 0.103 ± 0.021 is in agreement, inside the experimental uncertainty, with the value obtained from direct KX-ray measurement quoted above.

Studies on the Decay of ^{141}Ce

H.H.Hansen, E. Celen, D. Mouchel, A. Nylandsted-Larsen, R. Vaninbroukx, W. Zehner

The emitted electrons were recorded with a double focusing magnetic β spectrometer using a 5 mm thick plastic scintillator as detector. From the measured electron distribution plots of the two continuous β^- spectra have been constructed. The maximum energies, the relative intensities and the shape factors of both β^- spectra have been deduced. The results are shown in Table 4.1.

TABLE 4.1.

Results for ^{141}Ce decay

Deduced quantity	1. Branch $7/2^- \to 5/2^+$	2. Branch $7/2^- \to 7/2^+$
maximum β^- energy [keV]	581.9 ± 2.2	436.7 ± 0.8
relative intensity [%]	29.3 ± 0.8	70.7 ± 0.8
coefficient "a" of the shape factor $C(\epsilon) = 1 + a\,\epsilon$ ($\epsilon = E/m_o c^2 + 1$)	−(0.23± 0.04)	−(0.21± 0.03)

From the same electron recordings the intensity ratios of conversion electrons originating from different shells have been deduced. The results are K/L = 7.28 $\pm$ 0.07 and K/LM+ = 5.78 $\pm$ 0.05. All quoted uncertainties are standard deviations.
The emission rate of the K-shell internal conversion electrons has been determined from electron X-ray coincidence measurements. The X rays were detected with a high resolution Si(Li) probe and K-shell conversion electrons were recorded with the magnetic β spectrometer. Using in addition the disintegration rates of the sources as determined from 4 $\pi\beta$-γ coincidence experiments and relative γ-ray measurements, a preliminary value of the K-shell internal conversion probability could be deduced : $\kappa_K = 0.3106$. From this value together with the conversion ratio K/LM the conversion coefficient $\alpha_K = 0.384$ and $\alpha = 0.450$ have been obtained as preliminary results. Another value for the total internal conversion coefficient has been deduced from 4 $\pi\beta$- γ coincidence measurements by the efficiency extrapolation method to be $\alpha = 0.460$. Final results with definite error quotations will be available after careful consideration of pure β^- emitting ^{143}Pr contamination.

<u>Studies on the Decay of ^{241}Pu</u>

R. Vaninbroukx, J. Broothaerts, P. De Bièvre, B. Denecke, M. Gallet

The determination of the half-life of ^{241}Pu has been continued using the following methods:

1. Mass-spectrometric determination of the ^{241}Pu decay by measurements of the change in the $^{241}Pu/^{240}Pu$ ratio and the $(^{241}Pu/^{240}Pu)/(^{240}Pu/^{239}Pu)$ ratio of ratios as a function of time;

2. Measurement of the ^{241}Am ingrowth by α counting in a defined low geometry solid angle, and by γ counting using Si(Li) detectors, calibrated for the 60 keV line of ^{241}Am.

The Pu material used contained 92.7 % ^{241}Pu at the beginning of the measurements. The ^{241}Pu content of the samples used for the ^{241}Am-ingrowth measurements was determined by isotope-dilution mass spectrometry.
For the mass-spectrometric method the $^{241}Pu/^{240}Pu$ ratios and the $(^{241}Pu/^{240}Pu)/(^{240}Pu/^{239}Pu)$ ratios were measured four times over a

period of about 22 months. Before each measurement the ^{241}Am grown into the sample was separated from the Pu using ion-exchange techniques. Corrections for all known systematic effects have been applied, especially for isotope fractionation effects in the ion source in the case of the ^{241}Pu/^{240}Pu ratio determinations. This correction was determined by appropriate calibrations using three NBS Pu Reference Materials. In the ratio of ratios method these isotope fractionation effects cancel. The preliminary result of the measurements performed till now is 14.3 years ± 1 %. On request of the Atomic Energy Research Establishment (AERE), Harwell, measurements are proceeding on two different Harwell samples.

The short period of time between the two measurements performed on these materials does not yet allow to compute values for the half-life of ^{241}Pu with a reasonable accuracy. The isotopic composition of these materials has been measured very accurately and communicated to AERE. In the case of α counting a correction has to be applied for the contribution of the other Pu isotopes in the sample including the small α branch of ^{241}Pu. The amount of this contribution varied between 100 % at the time of separation and 5 % at the time of the final series of measurements about 20 months after the separation; 17 % of this contribution is due to the α branch of ^{241}Pu. In the case of γ counting a correction has to be applied for the contribution of ^{237}U, growing into the sample from the α decay of ^{241}Pu. This contribution varied between 35 % at the separation, and 1.5 % 14 months after the separation, where the measurements were stopped since the count rates became too high. The preliminary result obtained for the half-life of ^{241}Pu by the ^{241}Am in-growth method is 14.6 years ± 1 %.

The uncertainty on the intensity of the αdecay of ^{241}Pu to ^{237}U which decays with a half-life of 6.75 days to ^{237}Np mainly via the 60 keV level of ^{237}Np, influences the accuracy of γ-spectrometric ^{241}Am determinations in Pu samples. It also affects the accuracy of the mass determinations of Pu samples by α-counting techniques, especially when appreciable amounts of ^{241}Pu are present in the samples. Therefore, we redetermined the specific α emission of ^{241}Pu, yielding its partial α half-life, $T_{1/2}(\alpha)$. It was performed in three different ways: (1) by measuring during the first days after the separation, where the correction for tailing effects due to the ingrowing ^{241}Am is still small, the α-emission ratio ^{241}Pu/(^{239}Pu+^{240}Pu) using α-particle spectrometry; (2) via the 280 keV γ line in the decay of ^{237}U by γ-ray spectrometry using calibrated Ge(Li) and Si(Li) detectors, taking the γ-ray intensity ratio $I_\gamma(208)/I_\gamma(60)$=0.

from literature [13,14]; (3) via the measurement of the 60 keV γ-emission rate during the first days after the separation where the contribution of ^{241}Am could be calculated with sufficient accuracy. The results are shown in Table 4.2.

Table 4.2.

Specific α activity and a half-life of ^{241}Pu

Method	specific α emission s^{-1} / μg ^{241}Pu	$T_{1/2}(\alpha)$ years
α-Particle Spectrometry	91.3 ± 1.3	$(6.01 \pm 0.09)\times10^5$
γ-208 keV	90.6 ± 1.4	$(6.06 \pm 0.09)\times10^5$
γ-60 keV	90.9 ± 1.0	$(6.04 \pm 0.07)\times10^5$
Mean	90.9 ± 0.9	$(6.05 \pm 0.06)\times10^5$

Combination of the α half-life with a β half-life of 14.6 years yields the α intensity in the decay of ^{241}Pu: $I_\alpha = (2.42 \pm 0.02)\times10^{-5}$, in good agreement with the value of $(2.45 \pm 0.08)\times10^{-5}$ reported by Ahmad et al. [15].

Studies of the Decay of ^{239}Pu

R. Vaninbroukx, J. Broothaerts, P. De Bièvre, B. Denecke, M. Gallet, F. Hendrickx, F. Peetermans, J. Van Audenhove

The disintegration rate of five samples of a Pu material which contains 99.98 atom % have been determined by counting α particles in a defined solid angle of low geometry. The contribution of ^{240}Pu to the count rate was deduced to be 0.08 % from the isotopic composition of the sample which was determined by mass-spectrometric isotope analysis. The contribution of ^{238}Pu and ^{241}Am, if present, was measured by α - particle spectrometry to be 0.02 %. The ^{239}Pu content of the sample was determined by mass-spectrometric isotope dilution techniques. From these measurements the specific activity of ^{239}Pu could be deduced to be (2 298 ± 5) s^{-1} μg^{-1} yielding a half-life of ^{239}Pu of $(2.408 \pm 0.005)\cdot10^4$ years. This value and results from earlier measurements [4] on another Pu sample containing 97.62 atom % ^{239}Pu give a mean value for the half-life of ^{239}Pu of $(2.412 \pm 0.005)\cdot10^4$ years.

Study on the Decay of ^{241}Am

W. Bambynek, B. Denecke

Measurements to determine the intensity of the 60 keV γ rays in the ^{241}Am decay have been started. A 4 π scintillation spectrometer is used. It consists of two open CsI(Tl) crystals of 5 cm diameter and 2.5 cm thickness. These crystals have a hemispherical cavity of 1 cm diameter exactly in the center of the inner side of each crystal. The source is placed between the two detectors.
We have prepared sources by evaporation in vacuum onto 450 $\mu g/cm^2$ Mylar foils. The diameter of the sources is 3 mm. Ball-shaped absorbers were used to stop the α particles. Polyethylene of 0.05 mm thickness showed the best results. This material can be moulded to the required shape. It is optically transparent and will not prevent the detection of the escaping iodine KX rays and has a transmission of 0.999 for the γ rays of interest. These γ rays can be nicely separated from the N_p LX rays. Corrections have to be applied for the separation of the recorded lines of these radiations, for the deviation of the solid angle from 4 π and for the influence of dead layers on the surface of the detector crystals which deteriorate the resolution and give rise to additional absorption. The latter effect will be examined by a scanning apparatus which is under construction. To improve the results obtained sources with a diameter of 2 mm and source backings of smaller thickness (preferably 100 $\mu g/cm^2$) have to be prepared. The insensitive layers of the detectors will be removed by sputtering with Ar ions.

Determination of Half-Lives of ^{57}Co, ^{103}Ru and ^{109}Cd

R. Vaninbroukx, G. Grosse

Several sources of ^{57}Co, ^{103}Ru and ^{109}Cd were used for checking the long-term stability of the detection efficiency of Si(Li) detectors in the energy range between 10 keV and 25 keV e.g. for the half-life measurements on $^{93}Nb^m$ and for some preliminary investigations on the Rh KX ray self-absorption. As a check of the sources, they were re-measured at regular intervals over the whole period of observation with a 3" x 3" NaI(Tl) detector for which the long-term reproducibility is known as to be better than $\pm$ 0.05 %. As a byproduct these stability measurements were used for the calculation of the half-lives of these radionuclides. The measurements on ^{57}Co and ^{109}Cd will continue, those on ^{103}Ru are finished. The results are summarized in Table 4.3.

where the uncertainties stated are on the 99.73 % confidence level, taking into account random and systematic effects.

TABLE 4.3.

Half-Lives of ^{57}Co, ^{103}Ru, ^{109}Cd

Radionuclides	Period of observation in half-lives	Half-life (days)
^{57}Co	1.1	271.7 ± 0.8 *
^{103}Ru	3.4	39.26 ± 0.06
^{109}Cd	0.7	460 ± 4 *

* Preliminary values

Determination of Half-Lives of Low-Lying Nuclear Levels

A. Nylandsted-Larsen, D. Mouchel

A conventional slow-fast coincidence system has been built-up in order to determine short half-lives of low lying nuclear levels. It consists of a combination of two scintillators or one scintillator and one Si solid state detector associated with suitable fast electronics. As a test on the proper operation of the system the half-life of the first excited level in ^{119}Sn has been determined. The isomeric state at 89 keV in ^{119}Sn decays with a half-life of about 250 days by a highly converted M4 transition to the first excited level at 24 keV. This state is de-excited with a half-life of about 19 ns by a converted M1 transition. A special $^{119}Sn^{m}$ source has been prepared following the advice of G. Weyer and B. Bengtson, University of Aarhus, Denmark. The $^{119}Sn^{m}$ has been incorporated into a 0.2 mm thick NE 102A plastic scintillator. In such a way, this scintillator acts as source and as one of the detectors simultaneously.

The time resolution of the detection system has been found to be, respectively 9 ns and 1 ns, depending on whether a scintillator/Si(Li) detector or a two scintillator combination has been used. A preliminary value for the half-life of the 24 keV level in ^{119}Sn has been deduced being $T_{1/2}$ = 18.6 ns.

Determination of the Activity Ratio of $^{238}Pu/(^{239}Pu + ^{240}Pu)$ by α- Particle Spectrometry

G. Bortels, J. Broothaerts

The computer code to evaluate the $^{238}Pu/(^{239}Pu + ^{240}Pu)$ activity ratio in Pu samples by α-particle spectrometry has been improved. A better tailfit could be obtained. For sufficiently thin sources, which can easily be prepared with a suitable spreading agent the contribution of the ^{238}Pu low-energy tail to the $^{239}Pu + ^{240}Pu$ peaks is smaller than 5 % at 1.6 % abundance of ^{238}Pu. Under these conditions the uncertainty originating from the evaluation of the spectra contributes less than 0.2 % to the uncertainty of the activity ratio (Fig. 4.4.).

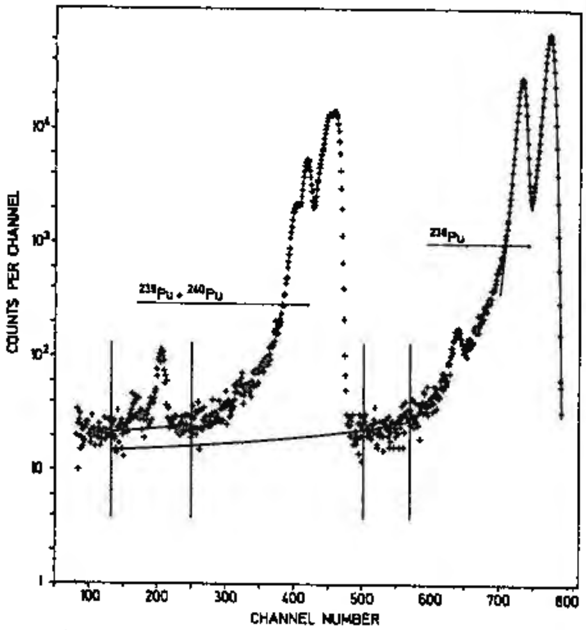

Fig. 4.4 Alpha ray spectrum of a Pu sample.

Compilation of Internal Conversion

H.H. Hansen

The literature search in order to establish a compilation of experimental results of internal conversion coefficients and ratios has been closed by December 1977. The study is made in collaboration with the Max-Planck-Institut für Kernphysik, Heidelberg and the Zentralstelle für Atomkernenergie Dokumentation, Karlsruhe. The work performed at CBNM was restricted to nuclides with $Z \leqslant 60$. About 680 publications have been retained and authors and references were quoted. Some 2500 transitions have been listed with energy, spin and parity of initial and final levels involved, and multipolarity. Values of 3600 internal conversion coefficients and 950 conversion ratios were extracted from the papers. In addition, for every transition the γ-ray emitting nucleus and its origin have been noted as well as the experimental methods used by the authors.

A draft of an introduction to the compilation has been written. It presents a summary on the internal conversion process, a description of the experimental methods applicable with an estimation of errors and a listing of the policies adopted for the tables.

Evaluation of Electron Capture Data

W. Bambynek

An extensive survey on "Orbital Electron Capture by the Nucleus" has been published [5]. The theory of nuclear electron capture is reviewed in the light of current understanding of weak interactions. Formulae and tables are provided that enable the reader to calculate transition rates and ratios of interest. Special attention is paid to electron-exchange and atomic wavefunction overlap effects on the transition probability. (Fig. 4.5. and Fig. 4.6.).
Experimental methods for the measurement of electron-capture probabilities and ratios and of electron-capture to β^+-emission ratios are described and compared.
Published data are listed, critically evaluated and compared with theory (Figs. 4.7. to 4.10.).

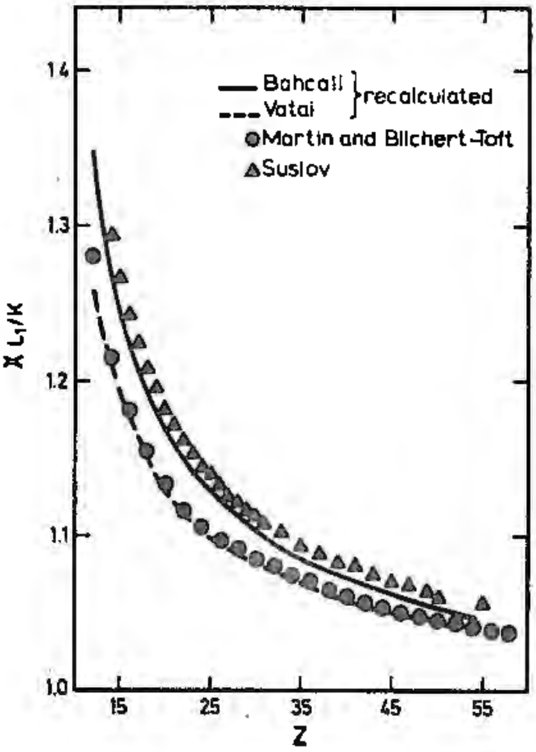

Figure 4.5. L_1/K exchange and overlap correction factors. The solid and broken curves were recalculated according to the approaches of Bahcall [6] and Vatai [7], respectively with wave functions from the Hartree-Fock program of Froese-Fischer [8] . Results of the relativistic calculation of Suslov [9] following Bahcall's theory, are indicated by triangles, and those of the calculation of Martin and Blichert-Toft [10] ,based on the same approach as Vatai's, are indicated by solid dots.

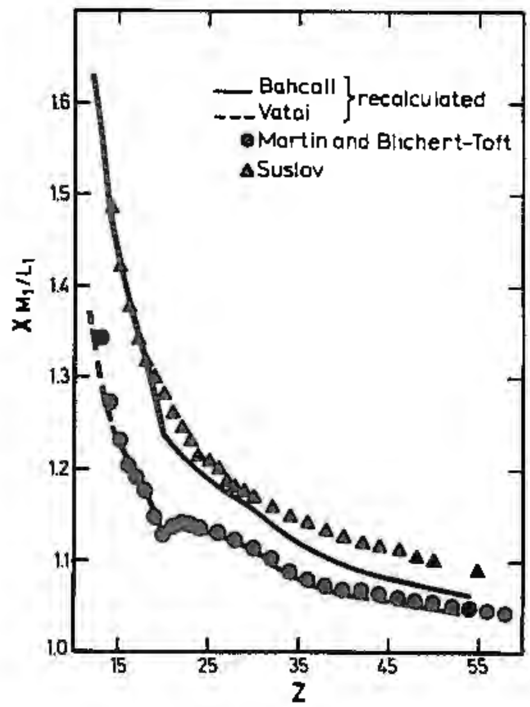

Fig. 4.6 M_1/L_1 exchange and overlap correction factors. See caption of fig 4.5 for details

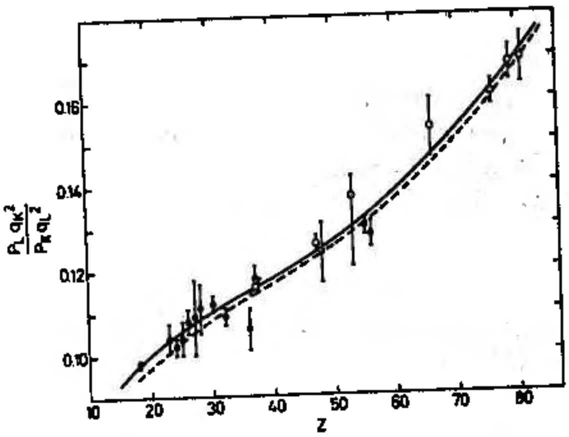

Figure 4.7. Comparison of experimentally determined L/K capture ratios for allowed transitions (solid circles) and first-forbidden non-unique transitions (open circles) with theoretical predictions based on wave functions of Mann and Waber [11] and exchange and overlap corrections $X^{L/K}$ according to Bahcall [6], Vatai [7] and Martin and Blichert-Toft [10].

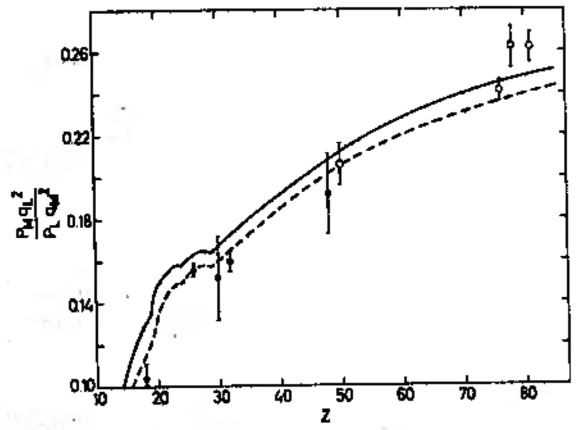

Fig.4.8 Comparison of experimentally determined M/L capture ratios for allowed transitions (solid circles) and first-forbidden non-unique transitions (open circles) with theoretical predictions (see caption of fig 4.7 for details)

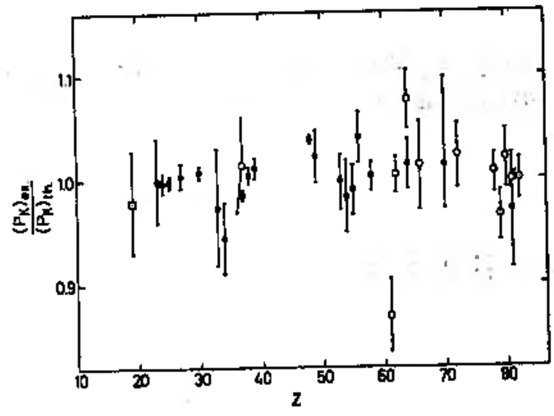

Fig.4.9 Comparison of experimentally determined P_K values for allowed transitions (solid circles), first-forbidden non-unique transitions (open circles), and first-forbidden unique transitions (squares) with theoretical predictions, (see caption of fig.4.7 for details).

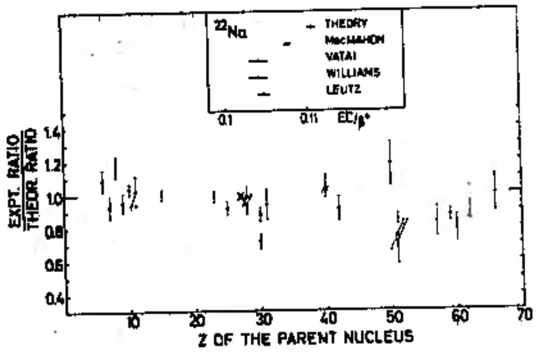

Fig. 4.10 Ratio of experimental to theoretical allowed K/β^+ and EC/β^+ ratios.

The theory of radiative electron capture and experimental work on internal bremsstrahlung are thoroughly reviewed and tables for the calculation of internal bremsstrahlung spectra are provided. A discussion of atomic transitions that accompany nuclear electron capture is included. A special effort is made at completeness in covering the subject. The survey will prove useful for both theoretical and experimental researchers.

REFERENCES

[1] K.A. KELLER, J. LANGE, H. MÜNZEL, G. PFENNIG
Landold-Börnstein, Numerical Data and Functional Relationships in Science and Technology, Q-Values and Excitation Functions of Nuclear Reactions (Springer Verlag, Berlin, 1973) Group I, Vol. 5, Part b.

[2] R. LLORET,
Mesure de la période de décroissance radioactive de $^{93}Nb^{m}$, Radiochem. Radioanal. Letters 29, 165 (1977).

[3] W. BAMBYNEK, B. CRASEMANN, R.W. FINK, H.-U. FREUND, HANS MARK, C.D. SWIFT, R.E. PRICE, P. VENUGOPALA RAO,
X-ray fluorescence yields, Auger, and Coster-Kronig transition probabilities, Rev. Mod. Phys. 44, 716 (1972).

[4] R. VANINBROUKX,
Half-Life of ^{239}Pu, in Review of Standard Reference Data and Important Cross Section Discrepancies, ANL/ND-77-1 (Argonne National Laboratory Report) 1976, p. 29.

[5] W. BAMBYNEK, H. BEHRENS, M.H. CHEN, B. CRASEMANN, M.L. FITZPATRICK, K.W.D. LEDINGHAM, H. GENZ, M. MUTTERER, E.L. INTEMANN,
Rev. Mod. Phys. 49, 77 (1977).

[6] J.N. BAHCALL,
Phys. Rev. 129, 2683 (1963, 131, 1956 (1963),
Nucl. Phys. 71, 267 (1965).

[7] E. VATAI,
Nucl. Phys. A 156, 541 (1970).

[8] C. FROESE-FISCHER,
Comput. Phys. Commun. 4, 107 (1972).

[9] Yu P. SUSLOV,
Izv. Acad. Nauk, SSSR, Ser. Fiz. 34, 79 (1970).

[10] M.J. MARTIN, P.H. BLICHERT-TOFT,
Nucl. Data A 8, 1 (1970).

[11] J.B. MANN, J.T. WABER,
Atomic Data 5, 201 (1973).

[12] R.S. HAGER, E.C. SELTZER,
Nucl. Data A4, 1 (1968).

[13] J.E. CLINE,
Idaho Nuclear Corporation Report IN-1448 Rev. (1971).

[14] R. GUNNINK, J.E. EVANS, A.L. PRINDLE,
UCRL-52139 (1976).

[15] I. AHMAD, A.M. FRIEDMAN, J.P. UNIK,
Nucl. Phys. A119, 27 (1968).

5. ACCELERATOR AND DETECTOR DEVELOPMENT

Realization of a Fission Chamber with Intrinsic Suppression of Alpha-Background

C. Budtz-Jørgensen, H.-H. Knitter

For the measurements of neutron-induced fission cross sections of highly alpha-active actinides, a new type of fission fragment detector was developed. The high specific activity of the nuclei under investigation, of 10^7 to 10^9 alphas $s^{-1}\cdot mg^{-1}$, demands special attention to pulse pile-up. Moreover, the detector must be very stable and have characteristics which are independent of radiation dose. The influence of pile-up can be reduced by choosing a detector with very fast response time and by reducing the detector pulse height of the alpha background radiation with respect to the wanted fission fragment signals. Ionisation chambers with flowing counter gas have proven to be very stable under high radiation dose. Although they are not the fastest type of detectors, the pile-up problem has been solved in the present design (1), which is based on the phenomenon that 5-6 MeV alpha-particles have a range in matter of about twice that of fission fragments. Fig. 5.1. shows the working principle of the detector.

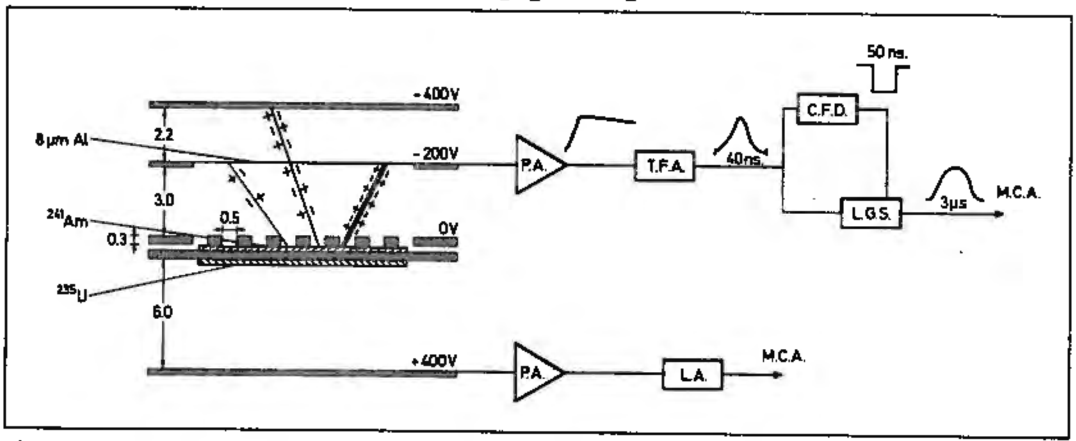

Fig. 5.1

Single layers of ^{235}U and ^{241}Am, 3 cm in diameter, are mounted back to back, such that both materials can be exposed to the same neutron flux. The lower half of the chamber is a normal parallel plate ionisation chamber and it is used for the detection of ^{235}U fission fragments. The ^{235}U fission cross section is used as a standard. Methane at NTP was used as counter gas because of its large electron drift velocity. The upper chamber, which is used to detect fission fragments from ^{241}Am, contains a middle electrode of 8 µm thick Am foil. The thickness is chosen such that fission fragments moving normal to the sample will just be stopped in the foil, whereas 8.1 MeV alpha-particles will pass the foil, stopping in the outer electrode. The distance between the three electrodes have been chosen such that the alpha-particles create nearly the same amount of ionisation charge in the two parts of the

chamber. Hence, under the influence of the electric fields, no net charge will flow to the middle electrode. That means: in principle, that no signal pulse will arise from the alpha particles. For the fission fragments of course the detector behaves as a normal parallel plate chamber.
In order to ensure that all alpha particles from the ^{241}Am sample will pass the middle electrode, a collimator, a 0.3 mm stainless steel plate with about 1500 holes of 0.5 mm diameter, is placed above the sample. The efficiency of the collimator was measured using weak ^{252}Cf and ^{241}Am sources. The precise metrological data of the collimator were determined with the help of a calibrated microscope. The collimator efficiency was calculated using these data, and a value was found which agreed to better than 2% with the measured ones. The typical efficiency of such a collimator is about 13%.
Commercially available charge sensitive preamplifiers are used. The rise-time of the fission induced signals is about 25 ns. The signals from the chamber with the high alpha background are shaped to pulses of less than 40 ns width using a timing filter amplifier. A fast linear gate, Ortec LG 105/N, is opened with a 50 ns wide gate pulse fed from a constant fraction discriminator. The stretched output from the linear gate is sorted in a multichannel analyzer. This type of ionisation chamber with intrinsic discrimination of alpha-background permits the measurement of neutron induced fission cross sections of actinides with a high specific alpha activity by fission fragment detection. It is used at the Van de Graaff and the electron linear accelerator of the CBNM for the measurement of the fission cross section of ^{241}Am [2].
In the subthreshold region a cross section as low as 20 mb could be measured having a clear separation between alpha-particle noise and fission fragments. It is expected that the chamber can operate with at least 5.10^{8} alphas s^{-1} passing the active chamber volume. Calculations show, that at this rate one would get less than 10^{-6} pile-up pulses per second above a threshold corresponding to 90% fission fragment detection efficiency. A detector with an active area of 9 cm diameter is under construction and will be loaded with 40 mg of ^{241}Am.

REFERENCES

[1] C. BUDTZ-JØRGENSEN, H.-H. KNITTER
NIM 154, 121 (1978)

[2] H.-H. KNITTER and C. BUDTZ-JØRGENSEN
to be published in ATKE

The Van de Graaff accelerators

A. Crametz, P. Falque, J. Leonard, R. Smets

Two vertical Van de Graaff accelerators can be operated simultaneously. The KN-3 MV Van de Graaff accelerator installed in 1963 and upgraded to 3.7 MV in 1973 produces fast monoenergetic neutrons in the ranges from 0.1 to 2.5 MeV, from 4.0 to 6.5 MeV and from 12.5 to 20 MeV. With H^+, D^+ or He^+ ions a DC beam of 30 μA, or a pulsed beam of 10 ns pulses at 1 MHz of 10 μA mean current is delivered by this accelerator.
Since January 1977, a vertical model CN-5.5 MV, upgraded to 7 MV, single stage Van de Graaff accelerator with klystron bunching is operational and produces fast monoenergetic neutrons in the ranges of energy from 0.1 to 10 MeV and from 12.5 to 24 MeV.
Either DC or pulsed beams of H^+, D^+ or He^+ ions can be produced. To generate short duration ion bursts, a beam is extracted from a radio frequency ion source; it is focused by an Einzel lens, analysed by a 30° magnet and swept across a chopping aperture to get pulses of 15-30 ns duration. This aperture is placed at the entrance of the klystron buncher tube to which a sinewave potential of frequency 15 MHz is applied.
Pulses as small as 1.5 ns FWHM at 3 MV and 1.25 ns at 7 MV with a pulse repetition rate of 2.5, 1.25 or 0.625 MHz may be obtained. The terminal voltage stability including ripple and drift is $\pm$ 2 kV. For a DC beam, the possible maximum current reaches 35 μA at 5 MeV and 20 μA at 1 and 7 MeV and for a pulsed beam 6 μA mean value at 2.5 MHz. This corresponds to a peak value of 1.5 mA.
After being accelerated and brought to a focus, the beam is deflected from the vertical to horizontal plane by a 90° magnet. The magnet has a mass-energy product of 24. The analysed beam is again focused by a quadrupole doublet lens and oriented by a switching magnet through one of the two connected beam tubes towards targets located in the target hall.

Electron Linear Accelerator

J.M. Salomé, R. Cools, R. Forni, F. Massardier, F. Menu, K. Meynants, P. Siméone, F. Van Reeth, C. Waller, J. Waelbers

The modernisation of the linear accelerator is completed. The new components are a 2 m long standing wave bunching section, two travelling wave sections, each 6 m long, an injection system with an 80 kV triode gun, and a 13 MW modulator for long pulses to drive the buncher.

The guaranteed parameters of the new machine are given in Table 5.1.

TABLE 5.1.

Characteristics of the Modernized Electron Linear Accelerator

	Short pulses (1)		Long pulses (2)		
burst width	4 ns	10 ns	100 ns	1 μs	2 μs
instantaneous current	9 A	9 A	1.5 A	0.22 A	0.22 A
repetition frequency	900 Hz	900 Hz	880 Hz	380 Hz	250 Hz
electron energy	120 MeV	105 MeV	87 MeV	100 MeV	100 MeV
beam power	3.9 kW	8.5 kW	11.5 kW	11 kW	11 kW

(1) For short pulses the maximum energy at small current is 130 MeV.

(2) For long pulses the maximum energy at small current is 150 MeV.

The final Linac acceptance tests were made in February 1977. From this time, the accelerator could continuously be operated with the parameters given in table 5.2. (March 1977 to June 1978).

TABLE 5.2.

Pulse length ns	Rep. rate Hz	Peak current A	Energy MeV	Time, hour	% of the time
4 to 5	800	9 to 10	110	1875	45%
10 to 20	400	10 to 6	100	1698	41%
20 to 30	100	6.5 to 4.5	100	430	10%
2000	250	0.12	32	20	0.5%
Miscellaneous	-	-	-	142	3.5%

Two stationary targets are used for neutron production. Both have the same geometry, a diameter of 30 mm and a mercury cooling system. One consists of natural uranium, the other of natural uranium with an enriched ^{235}U core. A mercury cooled rotary natural uranium target is designed to dissipate the increased beam power of the modernised Linac (14 kW). The cooling system composed of an electromagnetic pump and a mercury-air heat exchanger will rotate together with the target. 2000 A for the pump are supplied by sliding contacts. It is planned to test this target in 1978.

Some activation analysis experiments have been performed with an electron beam power of more than 1 kW on a water cooled platinum target. A magnetic deviation was installed in the target room to have the beam out of the main line. It is adjustable between 8 and about 40 MeV.

- - - - - -

6. CINDA ENTRIES

ELEMENT S	A	QUANTITY	TYPE	ENERGY MIN	MAX	DOCUMENTATION REF	VOL	PAGE	LAB	COMMENTS
LI	006	TOTAL	EXPT-PROG	10+5	70+5	INDC(EUR)	11	35	378 GEL	KNITTER+VDG TOF MEASM
LI	006	ELASTIC SCAT	EXPT-PROG	10+5	70+5	INDC(EUR)	11	35	378 GEL	KNITTER+OBTAINED BY INTEGER OF DEL
LI	006	DIFF ELASTIC	EXPT-PROG	10+5	70+5	INDC(EUR)	11	35	378 GEL	KNITTER+VDG TOF MEASM
LI	006	N, TRITON	COMP-PROG	10+2	20+7	INDC(EUR)	11	40	378 GEL	WATTECAMPS.RATIO TO B10(N,A)
B	010	TOTAL	COMP-PROG	10+2	20+7	INDC(EUR)	11	40	378 GEL	WATTECAMPS.(N,AO)+(N,A1)+BRANCH RAT
B	010	N,PROTON	COMP-PROG	10+2	20+7	INDC(EUR)	11	40	378 GEL	WATTECAMPS.(N,AO)+(N,A1)+BRANCH RAT
B	010	N,ALPHA	COMP-PROG	10+2	20+7	INDC(EUR)	11	40	378 GEL	WATTECAMPS.(N,AO)+(N,A1)+BRANCH RAT
B	010	N,ALPHA	EVAL-PROG	10+5	20+6	INDC(EUR)	11	42	378 GEL	LISKIEN+TBP
B	010	N,ALPHA	EXPT-PROG	10+2	20+6	INDC(EUR)	11	46	378 GEL	VIESTI+VDG TOF REL CURV TBP
FE		DIFF ELASTIC	EXPT-PROG	10+3	30+5	INDC(EUR)	11	15	378 GEL	BRUSEGAN+LINAC TOF MEASM
FE	054	N,GAMMA	EXPT-PROG	50+2	60+5	INDC(EUR)	11	15	378 GEL	BRUSEGAN+LINAC TOF MEASM
FE	056	TOTAL	EXPT-PROG	12+3		INDC(EUR)	11	15	378 GEL	BRUSEGAN+LINAC TOF MEASM
FE	056	N,GAMMA	EXPT-PROG	50+2	60+5	INDC(EUR)	11	15	378 GEL	BRUSEGAN+LINAC TOF MEASM
FE	056	RESON PARAMS	EXPT-PROG	12+3		INDC(EUR)	11	15	378 GEL	BRUSEGAN+LINAC TOF MEASM
NI		N,PROTON	EXPT-PROG	82+6	40+6	INSC(EUR)	11	8	378 GEL	PAULSEN+NP+NA DIR PART DETECT PRELIM
RH	103	TOTAL	EXPT-PROG	10+5	40+6	INDC(EUR)	11	5	378 GEL	PAULSEN+RH103M ACTIV MEASM
IN	115	TOTAL	EXPT-PROG	40+5	40+6	INDC(EUR)	11	5	378 GEL	LISKIEN+IN115M ACTIV MEASM
I	127	TOTAL	EXPT-PROG	20+1	20+3	INDC(EUR)	11	19	378 GEL	ROHR+LINAC TOF MEASM
I	127	N,GAMMA	EXPT-PROG	20+1	50+3	INDC(EUR)	11	19	378 GEL	ROHR+CAPT+SELF-INDICTN RATIO MEASM
I	127	RESON PARAMS	EXPT-PROG	20+1	20+3	INDC(EUR)	11	19	378 GEL	ROHR+
I	127	STRNTH FNCTN	EXPT-PROG	20+1	20+3	INDC(EUR)	11	19	378 GEL	ROHR+
I	127	LVL DENSITY	EXPT-PROG	20+1	20+3	INDC(EUR)	11	19	378 GEL	ROHR+
AU	197	N,GAMMA	THEO-PROG	10+4	10+6	INDC(EUR)	11	47	378 GEL	LISKIEN+CALC OF SIG FLUCTUATIONS

CINDA ENTRIES (continued)

ELEMENT S	A	QUANTITY	TYPE	ENERGY MIN	MAX	DOCUMENTATION REF VOLUME	PAGE	DATE	LAB	COMMENTS
TH	232	N,FISSION	EXPT-PROG	12+6	20+6	INDC(EUR)11	22	378	GEL	BLONS+LINAC TOF 2KEV RESOL
U	235	N,FISSION	EXPT-PROG	15-2	20+2	INDC(EUR)11	23	378	GEL	BARTHELEMY+REL TO LI6 AND B10(N,A)
U	235	N,FISSION	THEO-PROG	10+4	10+6	INDC(EUR)11	47	378	GEL	LISKIEN+CALC OF SIG FLUCTUATIONS
U	238	TOTAL	EXPT-PROG	10+0	43+3	INDC(EUR)11	27	378	GEL	CORNELIS+LINAC TOF MEASM
U	238	ELASTIC SCAT	EXPT-PROG	10+0	43+3	INDC(EUR)11	27	378	GEL	CORNELIS+LINAC TOF MEASM
U	238	N,GAMMA	EXPT-PROG	10+0	43+3	INDC(EUR)11	27	378	GEL	CORNELIS+LINAC TOF MEASM
U	238	RESON PARAMS	EXPT-PROG	67+0		INDC(EUR)11	24	378	GEL	STAVELOZ+SCAT EXPERIMENT
U	238	RESON PARAMS	EXPT-PROG	10+0	43+3	INDC(EUR)11	27	378	GEL	CORNELIS+LINAC TOF MEASM
U	238	STRNTH FNCTN	EXPT-PROG	10+0	43+3	INDC(EUR)11	27	378	GEL	CORNELIS+LINAC TOF MEASM
NP	237	TOTAL	EXPT-PROG	80+0	21+2	INDC(EUR)11	29	378	GEL	ANGELETTI+LINAC TOF MEASM
NP	237	ELASTIC SCAT	EXPT-PROG	80+0	21+2	INDC(EUR)11	29	378	GEL	ANGELETTI+LINAC TOF MEASM
NP	237	N,GAMMA	EXPT-PROG	80+0	21+2	INDC(EUR)11	29	378	GEL	ANGELETTI+LINAC TOF MEASM
NP	237	RESON PARAMS	EXPT-PROG	80+0	21+2	INDC(EUR)11	29	378	GEL	ANGELETTI+LINAC TOF MEASM
NP	237	STRNTH FNCTN	EXPT-PROG	80+0	21+2	INDC(EUR)11	29	378	GEL	ANGELETTI+LINAC TOF MEASM
NP	237	LVL DENSITY	EXPT-PROG	80+0	21+2	INDC(EUR)11	29	378	GEL	ANGELETTI+LINAC TOF MEASM
PU	239	FISS YIELD	EXPT-PROG	25-2	10+2	INDC(EUR)11	31	378	GEL	BARTHELEMY+MASS DISTRIB
PU	239	FRAG SPECTRA	EXPT-PROG	25-2	10+2	INDC(EUR)11	31	378	GEL	BARTHELEMY+KIN ENERGY SPECTRA
AM	241	N,FISSION	EXPT-PROG	50+3	50+6	INDC(EUR)11	31	378	GEL	BUDTZ-JOERGENSEN+VDG MEASM
AM	241	N,FISSION	EXPT-PROG	10+0	20+5	INDC(EUR)11	32	378	GEL	BUDTZ-JOERGENSEN+VLINAC TOF MEASM
AM	241	RESON PARAMS	EVAL-PROG	10+0	60+1	INDC(EUR)11	33	378	GEL	THEOBALD. AVERAGE WF CFD

7. LIST OF PUBLICATIONS

Only those publications of CBNM that are relevant to nuclear data, from January 1977 until August 1978

- Published

1. LISKIEN H., A. PAULSEN
   Neutron Yields of Light Elements under Alpha-Bombardment
   Atomkernenergie, Vol. 30, p. 59 (1977)

2. MITCHELL I., H.L. ESCHBACH
   Standards for Backscattering Analysis
   3rd Intern. Conf. on Ion Beam Analysis
   The Naval Research Lab. + Georgetown Univ., Washington D.C. (1977)
   Published in Nucl. Instr. & Meth. Vol. 149, p. 727 (1978)

3. CRAMETZ A.
   A Model CN-7 MV Van de Graaff Accelerator for the CBNM
   Physics Bulletin, Vol. 28, No. 5, p. 212 (1977)

4. KNITTER H.-H.
   Survey of Recent Experiments for the ^{7}Li-System
   Intern. Specialists Symposium on Neutron Standards and Applications
   N.B.S. Gaithersburg, USA, p. 3 (1977)

5. PAULSEN A.
   Utility and Use of Neutron Capture Cross Section Standards and the Status of the Au(n,γ) Standard
   Proc. of Intern. Specialists Symposium on Neutron Standards and Applications, NBS Gaithersburg, USA
   NBS Publication 493 (1977)

6. WATTECAMPS E.
   Review of $^{10}B(n,\alpha)^{7}Li$ Cross-Section Measurements in the Energy Range from 10 keV to 1 MeV
   Proc. of Intern. Specialists Symposium on Neutron Standards and Applications, NBS Gaithersburg, USA
   NBS Publication 493, p. 6 (1977)

7. LE DUIGOU Y., W. LEIDERT
   Mechanism of a secondary reaction during the coulometric determination of uranium in a mixture with iron
   Z. Anal. Chem. 289, p. 279 (1978)

8. VAN AUDENHOVE J., P. DE BIEVRE, J. PAUWELS
   Fission Foils and Alloys containing Fissile Materials prepared at CBNM
   Proc. of ASTM-Euratom Symposium Palo-Alto (1977)

9. BUDTZ-JØRGENSEN C., KNITTER H.-H.
   A Fission Chamber with intrinsic Suppression of Alpha Background
   Nucl. Instr. and Methods, Vol. 154, p. 121 (1978)

10. BAMBYNEK W., I.V. MITCHELL, H. WEIGMANN
    Central Bureau for Nuclear Measurements
    Europhysics News, Europhysical Society, Vol. 9, No. 5, p. 1 (1978)

11. VANINBROUKX R.
Determination of Pu-241 in Am-241 by Gamma-Ray Spectrometry
International Journal of Applied Radiation and Isotopes,
Vol. 29, p. 379 (1978)

12. PAULSEN A.
Status Report about some Activation, Hydrogen and Helium Producing Cross-Sections of Structural Materials.
Proc. of Specialists Meeting on Neutron Data of Structural Materials for Fast Reactors, p. 261, CEC-JRC Geel (1977)

13. BRUSEGAN A., F. CORVI, G. PASQUARIELLO, G. ROHR, R. SHELLEY, T. VAN DER VEEN, E. CORNELIS, L. MEWISSEN, F. POORTMANS
Neutron Transmission and Capture Measurements of Separated Fe Isotopes.
Proc. of Specialists Meeting on Neutron Data of Structural Materials for Fast Reactors, p. 606, CEC-JRC Geel (1977)

14. ROHR G.
Evaluation and Calculation of Some Average Resonance Parameters for Structural Materials.
Proc. of Specialists Meeting on Neutron Data of Structural Materials for Fast Reactors, p. 614, CEC-JRC Geel (1977)

15. WEIGMANN H., J.A. HARVEY, R.L. MACKLIN, S. RAMAN, G.G. SLAUGHTER
Resonance Parameters, Capture γ-Rays and Reaction Mechanism in $^{98,100}Mo$ + n.
Proc. of Specialists Meeting on Neutron Data of Structural Materials for Fast Reactors, p. 739, CEC-JRC Geel (1977)

16. STAVELOZ P., F. POORTMANS, L. MEWISSEN, E. CORNELIS
Precise Measurements of the Capture Width of the 6.67 eV Neutron Resonance of Uranium-238.
Nucl. Sci. and Eng. 66, 349-353 (1978)

17. BAMBYNEK W., H. BEHRENS, M.H. CHEN, B. CRASEMANN, M.L. FITZPATRICK, K.W.D. LEDINGHAM, H. GENZ, M. MUTTERER, R.L. INTEMANN.
Orbital Electron Capture by the Nucleus.
Rev. Mod. Phys. Vol. 49, p. 77 and p. 961 (1977)

18. STEFANON M., F. CORVI
Resonance Neutron Capture Gamma Rays in $^{177}Hf^{+}$
Nuclear Physics A281, p. 240 (1977)

19. DE BIEVRE P.
Accurate Isotope Ratio Mass Spectrometry: Some Problems and Possibilities.
Proc. of the Int. Mass Spectrometry Conf. Florence, p. 385 Publ.(1978)

20. DEBUS G.H.
Programme Progress Report July - Dec. 1977 of METRE,
C.E.C. - JRC Geel

21. DEBUS G.H.
Final Report of JRC 1973-1976 Programmes, C.E.C.-JRC, Geel

- Submitted for Publication

1. LISKIEN H., E. WATTECAMPS
   Best values for the cross sections of the neutron standard reaction $^{10}B(n,\alpha)^{7}Li^{*}$ in the 0.1 to 2 MeV range
   Nucl.Sc. and Eng., submitted for publication (1977)

2. BENSUSSAN A., J.M. SALOME
   Gelina, A Modern Accelerator High Resolution Neutron Time of Flight Experiments.
   Nucl. Instr. and Methods, submitted for publication (1978)

3. LISKIEN H., F. ARNOTTE, R. WIDERA, A. PAULSEN
   Cross Section Measurement for the Reaction In-115(m,n')In^{m}-115
   Nucl. Sc. and Eng., submitted for publication (1978)

4. BASTIAN C.
   Discrimination of Counting Fluctuations in Multichannel Spectra
   Nucl. Instr. and Methods, submitted for publication (1978)

5. MITCHELL I.V., W. DOBMA
   Simple, Robust and Accurate Model Making of UHV Systems
   Journal of Vacuum Science and Technology, submitted for publication (1978)

6. BERTHELOT CH., G. CARRARO, V. VERDINGH
   The Use of Photon Activation for the Determination of Sm, Eu, Gd, and Dy in Boron Carbide
   5th Symp. on the Recent Dev. in Activation Analysis.
   St. Cath. Coll. Oxford, submitted for publication in
   J. Radioanalyticae Chem. (1978)

7. PAUWELS J.
   The contribution of nuclear analysis methods to the certification of BCR reference for non-metals in non-ferrous metals.
   5th Symposium on the Recent Developments in Activation Analysis.
   Oxford, Paper 64 (1968)

8. BARFOOT K.M., I.V. MITCHELL, H.L. ESCHBACH, P.I. MASON and W.B. GILBOY
   The Combined Use of Ion Induced X-ray Emission and Rutherford backscattering in the Analysis of Thin Environmental Samples.
   5th Conf. on the Recent Development in Activation Analysis,
   AERE Harwell and CBNM Geel. Oxford.
   Submitted for publication in J. Radioanalyticae Chem. (1978)

9. MASON P.I., W.B. GILBOY, K.M. BARFOOT, I.V. MITCHELL, H.L. ESCHBACH
   PIXE Analysis of Time Resolved Aerosol Samples.
   5th Conf. on the Recent Development in Activation Analysis,
   AERE, Harwell and CBNM Geel (1978).

10. MITCHELL I.V., K.M. BARFOOT, H.L. ESCHBACH
    The use of thin reference foils to calibrate ion beam experiments.
    5th Conf. on Recent Development in Activation Analysis,
    AERE Harwell and CBNM Geel.
    To be published in Nucl.Instr. & Meth. (1978)

11. DE BIEVRE P.
    Isotope Dilution of the Actinide Elements.
    Proc. of Annual Meeting, American Society for Mass Spectrometry,
    St. Louis, Mo (1978), to be published.

12. VIESTI G., H. LISKIEN
The $^{10}B(n,\alpha)^{7}Li$ Cross Section between 0.1 and 2.2 MeV
Annals of Nuclear Energy, submitted for publication (1978)

13. DOBMA W., H.L. ESCHBACH
Rotable support for the evaporation of boron in ultrahigh vacuum.
Vacuum, London, submitted for publication (1978)

14. WEIGMANN H., S. RAMAN, J.A. HARVEY, R.L. MACKLIN and G. SLAUGHTER
Capture γ-Rays and Reaction Mechanism in ^{100}Mo + n.
Proc. of Third Int. Symp. on Neutron Capture Gamma Ray Spectroscopy and Related Topics.
Brookhaven, 18-22 Sept., 1978

15. LISKIEN H.
The Particles Spectrum to be expected from a d-t Plasma.
Submitted for publication (1978)

16. KNITTER H.-H., C. BUDTZ-JØRGENSEN
Measurement of the Neutron Fission Cross Section of 241-Am from 100 eV to 5.3 MeV
Atomkernenergie, submitted for publication (1978)

17. KNITTER H.-H., C. BUDTZ-JØRGENSEN
Measurement of the ^{241}Am neutron induced fission cross section in the energy range from 100 eV to 5.3 MeV.
Int. Conf. on Neutron Physics and Nuclear Data for Reactors and Other Applications, AERE Harwell (1978)

18. ROHR G., R. SHELLEY
A New Interpretation of the Level Density Systematics
Int. Conf. on Neutron Physics and Nuclear Data for Reactors and Other Applications.
AERE Harwell (1978)

19. VANINBROUKX R.
New Determination of the Half-Life of Pu-241.
Int. Conf. on Neutron Physics and Nuclear Data for Reactors and Other Applications, AERE Harwell (1978)

20. BAMBYNEK W., D. REHER, R. VANINBROUKX
Decay of $^{93}Nb^{m}$
Int. Conf. on Neutron Physics and Nuclear Data for Reactors and other Applications, AERE Harwell (1978)

21. WEIGMANN H.
Measurement of the Cross-Sections of the Minor Transactinium Isotopes.
Proc. of Int. Conf. on Nuclear Physics and Neutron Data for Reactors and Other Applications, AERE Harwell, Sept. (1978)

22. MEWISSEN L., F. POORTMANS, E. CORNELIS, G. VANPRAET, A. ANGELETTI, G. ROHR, H. WEIGMANN.
Neutron Resonance Parameters for ^{237}Np.
Submitted for publication to Nucl.Sci. and Eng. (1978)

23. BLONS J., C. MAZUR, D. PAYA, M. RIBRAG, H. WEIGMANN
Rotational Bands in Asymmetrically Deformed ^{231}Th.
Submitted for publication to Phys. Rev. Letters (1978)

24. WEIGMANN H., P. MANAKOS
Deuteron Exchange Mechanism for the $^6Li(n,\alpha)$ Reaction at Low Energies.
Z. Physik, submitted for publication (1978)

25. ROHR G.
Statistical Model Calculation of the Total Radiative Width and the Degree of Freedom in the Capture Process.
Contribution to the "Third Int. Symp. on Neutron Capture Gamma Ray Spectroscopy and Related Topics,"Brookhaven Nat. Lab. (1978)

26. ROHR G., R. SHELLEY
A New Interpretation of the Level Density Systematics.
Proc. of Int. Conf. on Neutron Physics and Nuclear Data for Reactors and other Applied Purposes, AERE Harwell, Sept. 1978.

27. WINTER J., G. ROHR, R. SHELLEY, T. VAN DER VEEN, E. CORNELIS, L. MEWISSEN, F. POORTMANS, G. VAN PRAET
Neutron Cross-Sections Below 7 keV for ^{93}Nb.
Int. Conf. on Neutron Physics and Nuclear Data for Reactors and other Applications, AERE Hawrell, 1978

28. STAVELOZ P., E. CORNELIS, L. MEWISSEN, F. POORTMANS
Neutron Resonance Parameters of ^{105}Pd and ^{108}Pd.
Int. Conf. on Neutron Physics and Nuclear Data for Reactors and Other Applications, AERE-Harwell (1978).

29. BRUSEGAN A., F. CORVI, G. ROHR, C. COCEVA, P. GIACOBBE, M. MAGNANI
Neutron Resonance Parameters of ^{91}Zr.
Int. Conf. on Neutron Physics and Nuclear Data for Reactors and Other Applications, AERE-Harwell (1978)

30. CORVI F., G. PASQUARIELLO, T. VAN DER VEEN.
p-Wave Assignments of ^{232}Th Neutron Resonances.
Int. Conf. on Neutron Physics and Nuclear Data for Reactor and other Applications.
AERE-Harwell (1978)
